Connecting the Greenland ice-core and U/Th timescales via cosmogenic radionuclides: Testing the synchroneity of Dansgaard-Oeschger events

Florian Adolphi[1,2], Christopher Bronk Ramsey[3], Tobias Erhardt[1], R. Lawrence Edwards[4], Hai Cheng[4,5], Chris S. M. Turney[6], Alan Cooper[7], Anders Svensson[8], Sune O. Rasmussen[8], Hubertus Fischer[1] and Raimund Muscheler[2]

[1]Climate and Environmental Physics, Physics Institute & Oeschger Centre for Climate Change Research, University of Bern, Sidlerstrasse 5, 3012 Bern, Switzerland
[2]Quaternary Sciences, Department of Geology, Lund University, Sölvegatan 12, 22362 Lund, Sweden
[3]Research Laboratory for Archaeology and the History of Art, University of Oxford, Dyson Perrins Building, South Parks Road, Oxford OX1 3QY, UK
[4]Insitute of Global Environmental Change, Xi'an Jiatong University, Xi'an 710049, China
[5]Department of Erath Sciences, University of Minnesota, Minneapolis, Minnesota, 55455, USA
[6]Palaeontology, Geobiology and Earth Archives Research Centre and ARC Centre of Excellence in Australian Biodiversity and Heritage, School of Biological, Earth and Environmental Sciences, University of New South Wales, Sydney, NSW 2052, Australia
[7]Australian Centre for Ancient DNA and ARC Centre of Excellence in Australian Biodiversity and Heritage, School of Biological Sciences, The University of Adelaide, Adelaide, SA 5005, Australia
[8]Centre for Ice and Climate, Niels Bohr Institute, University of Copenhagen, Juliane Maries Vej 30, 2100 Copenhagen, Denmark

Correspondence to: Florian Adolphi (adolphi@climate.unibe.ch)

Abstract. During the last glacial period Northern Hemisphere climate was characterized by extreme and abrupt climate changes, so-called Dansgaard-Oeschger (DO) events. Most clearly observed as temperature changes in Greenland ice-core records, their climatic imprint was geographically widespread. However, the temporal relation between DO-events in Greenland and other regions is uncertain due to the chronological uncertainties of each archive, limiting our ability to test hypotheses of synchronous change. On the contrary, the assumption of direct synchrony of climate changes forms the basis of many timescales. Here, we use cosmogenic radionuclides (^{10}Be, ^{36}Cl, ^{14}C) to link Greenland ice-core records to U/Th-dated speleothems, quantify offsets between both timescales, and improve their absolute dating back to 45,000 years ago. This approach allows us to test the assumption that DO-events occurred synchronously between Greenland ice-core and tropical speleothem records at unprecedented precision. We find that the onset of DO-events occurs within synchronization uncertainties in all investigated records. Importantly, we demonstrate that there remain local discrepancies in the temporal development of rapid climate change for specific events and speleothems. These may be either related to the location of proxy records relative to the shifting atmospheric fronts or to underestimated U/Th-dating uncertainties. Our study thus highlights the potential for misleading interpretations of the Earth system when applying the common practice of climate wiggle-matching.

1 Introduction

Precise and accurate chronologies are critical for understanding past environmental and climatic changes. Global natural and anthropogenic archives can only be directly compared through the development of robust

chronological frameworks, enabling studies of the spatiotemporal dynamics of past change. These findings are crucial for understanding the nature and cause of rapid climate changes in the past, and hence, characterizing the dynamics and feedbacks of past and projected future climate change (Thomas, 2016). However, the applicability, precision, and accuracy of the available dating methods pose strong constraints on our ability to infer leads and lags between climate records, and ultimately, mechanisms of change in the Earth system. Instead, the situation is often reversed: climate changes such as Dansgaard-Oeschger, or DO, events (Dansgaard et al., 1993; Dansgaard et al., 1969) are typically *assumed* to occur synchronously across the Northern Hemisphere in different climate proxies from various regions and then used as chronological tie-points. This so-called "climate wiggle-matching" forms the chronological basis of a large part of paleoclimate records (e.g., Bard et al., 2013; Hughen et al., 2006; Henry et al., 2016; Turney et al., 2015), especially in the marine realm where other dating methods suffer from low precision and poorly constrained biases such as the marine radiocarbon reservoir age (Lougheed et al., 2013). Furthermore, it also plays a central role for one of the most widely used dating methods in paleosciences – the radiocarbon dating method. The current radiocarbon dating calibration curve (IntCal13, Reimer et al., 2013) is constructed from accurately dated tree-ring chronologies back to 13.9 ka BP (13.9 ka BP, kilo-years Before Present AD 1950). Beyond this time, which encompasses all DO-events, about one fourth of the data underlying IntCal13 obtain their absolute age from climate wiggle-matching.

Climate wiggle-matching has the obvious drawback that the leads and lags between different climate records cannot be studied once the records have been forced to align. The approach critically rests on the assumptions, that i) the climate change indeed occurred synchronously everywhere, and that ii) the (sometimes fundamentally different) proxies in question record the changes in a similar way and without intrinsic delays. These assumptions, however, can very rarely be rigorously tested but when they are, ample evidence is revealed that questions their universal validity. Lane et al. (2013) showed that rapid climate change in the North Atlantic region may be time transgressive with regional leads and lags on the order of a century. Nakagawa et al. (2003) argued that the onset of Greenland Interstadial 1e (GI-1e, Rasmussen et al., 2014a) occurred multiple centuries after the associated climate shift in Japan (and subsequent revisions of the underlying timescales (Staff et al., 2013; Bronk Ramsey et al., 2012; Seierstad et al., 2014) did not resolve this conundrum). Buizert et al. (2015) inferred that the Southern Ocean response to DO-events is delayed by about 200 years on average while the atmosphere around Antarctica reacted instantaneously (Markle et al., 2016). Baumgartner et al. (2014) found asynchronicities between ice-core proxies for local Greenland temperature (δ^{15}N) and the tropical/mid-latitude hydrological cycle (CH_4) during some DO-events. They discussed that the climate changes in polar and low-latitude regions may indeed be synchronous, but that atmospheric CH_4 concentrations rise with a delay during some DO-events because of compensating changes in the source strengths of the northern and southern hemisphere wetlands. Alternatively, their findings can be explained via a real delay between Greenland climate change and the activation of CH_4 source areas during certain DO-events. Fleitmann et al. (2009) reported on timing differences of DO-events in Greenland ice cores and speleothems, albeit largely within dating uncertainties. However, they also found significant differences between speleothem records outside their chronological uncertainties. This is complemented by a recent study showing that the duration of a stadial-interstadial transition can differ by up to 300 years between different East Asian speleothems (Li et al., 2017)

79 emphasizing the questions of whether we should expect the onset, mid-point, or end-point of DO-events to
80 occur simultaneously, as this choice will lead to different results when aligning the records.

81 In this paper, we attempt to provide improved constraints on the paradigm of climate synchroneity. We employ
82 cosmogenic radionuclides as a climate-independent synchronization-tool between the Greenland ice-core
83 timescale (Andersen et al., 2006; Rasmussen et al., 2006; Seierstad et al., 2014; Svensson et al., 2008; Svensson
84 et al., 2006; Vinther et al., 2006) and the U/Th timescale (Broecker, 1963; Edwards et al., 1987; Cheng et al.,
85 2013a) and strongly reduce the absolute dating error of the Greenland ice cores back to 45,000 years BP. This
86 allows us to compare the timing of DO-type variability seen in key paleoclimate records at unprecedented
87 precision: The Greenland ice cores and U/Th-dated (sub-)tropical speleothems.

88 **2 Cosmogenic radionuclides as synchronization tools**

89 Cosmogenic radionuclides (such as ^{14}C, ^{10}Be and ^{36}Cl) are produced in a nuclear cascade that is triggered when
90 galactic cosmic rays (GCR) collide with the Earth's atmosphere's constituents (Lal and Peters, 1967). While the
91 GCR flux outside the heliosphere can be assumed to be constant over the past million years (Vogt et al., 1990),
92 the flux arriving at Earth is modulated by the strength of the helio- and geomagnetic fields (Masarik and Beer,
93 1999). This causes the production rates of cosmogenic radionuclides to be inversely related to changes in solar
94 activity and/or the strength of the geomagnetic field. This modulation effect leaves a globally synchronous,
95 externally forced signal in cosmogenic radionuclide records around the world. Hence, they can serve as a
96 powerful synchronization tool for climate archives from different regions. The challenge lies in estimating
97 potential non-production-related impacts on radionuclide concentrations in a given archive that may result from
98 geochemical and meteorological processes.

99 After production, ^{14}C is oxidized to $^{14}CO_2$ and enters the carbon cycle. Changing ^{14}C production rates thus alter
100 the atmospheric $^{14}C/^{12}C$ ratio (expressed as per mille Δ^{14}C, that is, $^{14}C/^{12}C$ corrected for fractionation and decay
101 relative to a standard, denoted Δ in Stuiver & Pollach, 1977). Due to carbon cycle effects, these variations in
102 Δ^{14}C are dampened and delayed with respect to the causal production rate changes (Siegenthaler et al., 1980;
103 Roth and Joos, 2013). In addition to variable production rates, changes in the exchange rates between the
104 different carbon pools can alter Δ^{14}C. The world's oceans in particular have a significantly lower Δ^{14}C than the
105 contemporary atmosphere due to their long carbon residence time (Craig, 1957). Thus, variations in the ^{14}C
106 exchange rates between the ocean and the atmosphere will alter atmospheric Δ^{14}C independent of production
107 rate changes.

108 ^{10}Be attaches to aerosols and is transported from the stratosphere to the troposphere within 1-2 years (Raisbeck
109 et al., 1981) mainly via mid-latitude tropopause breaks (Heikkilä et al., 2011). It has no active geochemical
110 cycle and so its atmospheric concentration is a more direct recorder of production rate changes compared with
111 Δ^{14}C. However, ^{10}Be transport and deposition in the troposphere is guided by local meteorology and thus
112 susceptible to changes thereof (Heikkilä and Smith, 2013; Pedro et al., 2011). This can cause variations in ^{10}Be
113 records that are not related to production rate changes. Furthermore, a so-called "polar bias" (i.e., an
114 overrepresentation of polar as opposed to global production rate changes) has been proposed for ice-core records
115 (Bard et al., 1997). This would lead to subdued geomagnetic and enhanced solar modulation of ice-core
116 radionuclide records due to the geometry of the geomagnetic field. However, there is no consensus in different

117 empirical studies and modelling experiments to whether this effect is present and the results may also vary
118 regionally (Bard et al., 1997; Heikkilä et al., 2009a; Pedro et al., 2012; Adolphi and Muscheler, 2016;
119 Muscheler and Heikkilä, 2011; Field et al., 2006).

120 The transport and deposition of ^{36}Cl in its aerosol phase is comparable to ^{10}Be. However, in addition to an
121 aerosol phase, ^{36}Cl also has a gaseous phase (H^{36}Cl) which is likely dominant in the stratosphere (Zerle et al.,
122 1997). In the troposphere, the partitioning between aerosol and gas phase is not well understood. It may vary in
123 space and time (Lukasczyk, 1994), and can change rapidly depending on pH (Watson et al., 1990). The gaseous
124 H^{36}Cl phase can also be lost from acidic ice in low accumulation sites after deposition which is, however, less
125 relevant for the high accumulation sites studied here (Delmas et al., 2004). In Greenland, similar to ^{10}Be, the
126 dominant deposition process of ^{36}Cl in is wet deposition (Heikkilä et al., 2009b) which is supported by the
127 overall similarity of ^{36}Cl and ^{10}Be variations recorded in ice cores (Wagner et al., 2001b; Muscheler et al.,
128 2005).

129 As a result, all three radionuclides depend on the same production mechanism which causes their production
130 rates to co-vary globally. This signal can be exploited for global synchronization of paleorecords from natural
131 archives. However, to identify these common changes, their different geochemistry needs to be accounted for. In
132 the case of radiocarbon this is achieved through carbon cycle modelling, to deconvolve the effects of the carbon
133 cycle on the relation between ^{14}C production rates and Δ^{14}C (Muscheler et al., 2004). For ^{10}Be and ^{36}Cl, fluxes
134 can be calculated from ice accumulation rates. This provides a first-order correction for changing
135 paleoprecipitation rates on the ice sheet and their influence on the radionuclide concentrations. In reality, aerosol
136 transport to the ice sheet is more complex and depends on changes in transport velocity, pathways and
137 scavenging effects en route (Schüpbach et al., 2018), which are, however, difficult to constrain for ^{10}Be due to
138 its stratospheric origin. Instead, comparisons of fluxes and concentrations to other climate proxies can inform
139 about potential climate influences on ^{10}Be and^{36}Cl transport and deposition (Adolphi and Muscheler, 2016). It is
140 currently not possible to quantitatively correct either of the radionuclides for these non-production influences
141 since neither past carbon cycle changes nor atmospheric circulation changes are sufficiently well known.
142 However, the potential amplitude of non-production rate changes can be assessed through sensitivity
143 experiments and added as an uncertainty for the production rate signal (Adolphi and Muscheler, 2016; Köhler et
144 al., 2006).

145 The potential of this synchronization tool has been demonstrated multiple times to infer differences between the
146 tree-ring and ice-core timescales (Adolphi and Muscheler, 2016; Muscheler et al., 2014a; Southon, 2002), test
147 the accuracy of the radiocarbon calibration curve (Adolphi et al., 2017; Muscheler et al., 2014b; Muscheler et
148 al., 2008), and synchronize ice cores from both hemispheres (Raisbeck et al., 2017; Raisbeck et al., 2007).

149 **3 Methods & Data**

150 **3.1 Ice-Core Data**

151 The ice-core ^{10}Be and ^{36}Cl data used in this study are shown in figure 1. We focus on records that have been
152 robustly linked to the GICC05 timescale (Andersen et al., 2006; Rasmussen et al., 2006; Seierstad et al., 2014;

153 Svensson et al., 2008; Rasmussen et al., 2008). Hence, the majority of the data stems from the deep Greenland

154 ice cores GRIP, GISP2, and NGRIP. In addition, we use Antarctic ^{10}Be fluxes from EDC, EDML and Vostok

155
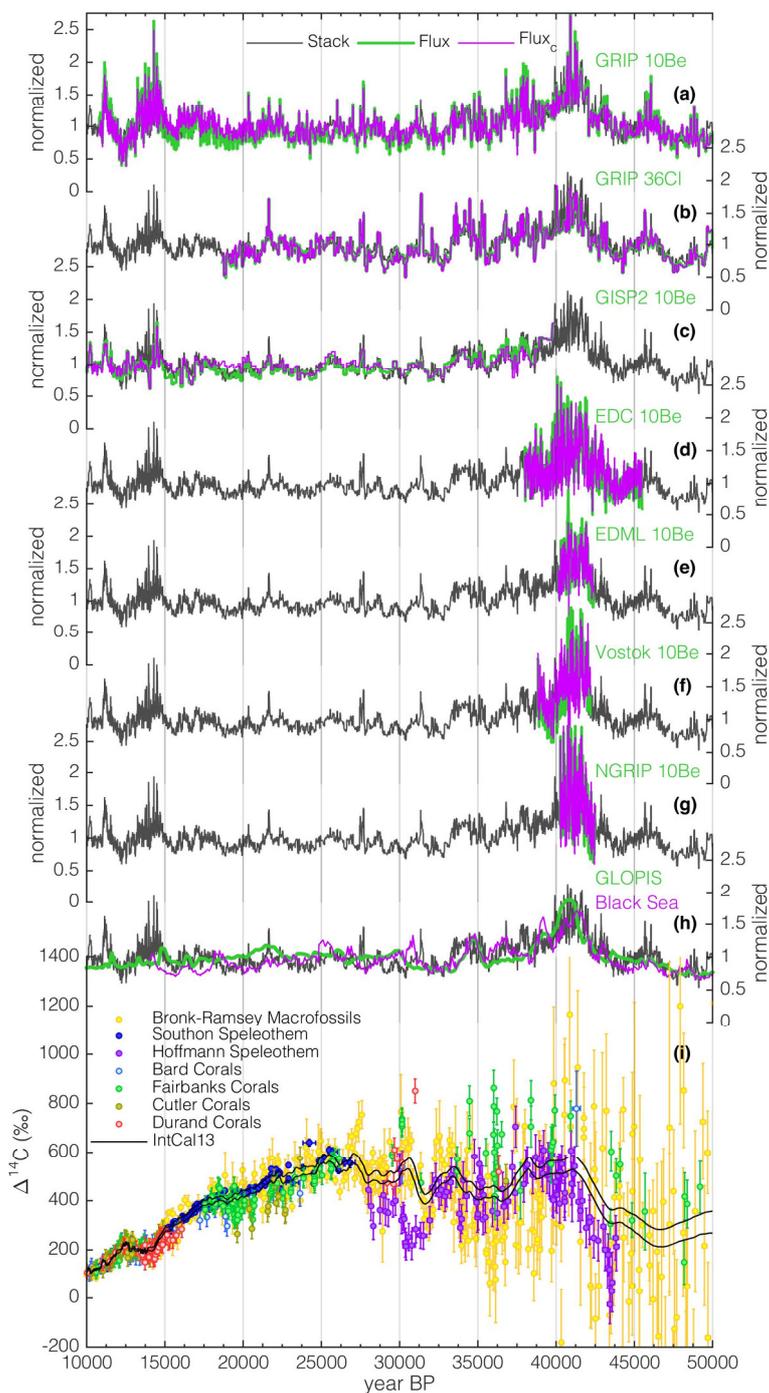
Figure 1: Data used in this study. Panel a-g show individual ice-core records of GRIP ^{10}Be (Baumgartner et al., 1997b; Muscheler et al., 2004; Wagner et al., 2001a; Yiou et al., 1997; Adolphi et al., 2014), GRIP ^{36}Cl (Baumgartner et al., 1998; Baumgartner et al., 1997a; Wagner et al., 2001b; Wagner et al., 2000), GISP2 ^{10}Be (Finkel and Nishiizumi, 1997), and ^{10}Be from EDC, EDML, Vostok, and NGRIP (all Raisbeck et al., 2017). Each record represents deposition fluxes (green) and 'climate corrected' fluxes (purple, see text). In addition, each panel contains the stack of all ice-core records (black, see text). Panel h: ^{10}Be production rates modelled from two geomagnetic field intensity reconstructions: GLOPIS (green, Laj et al., 2004) and based on Black Sea sediments (purple, Nowaczyk et al., 2013) using the production rate model by Herbst et al. (2016). The ice-core radionuclide stack is shown in black. All records in panel a-h are shown on the GICC05 timescale (Seierstad et al., 2014) and normalized to (i.e., divided by) their mean. Panel i: Absolutely dated ^{14}C data from Lake Suigetsu (yellow, Bronk Ramsey et al., 2012), Hulu Cave (blue, Southon et al., 2012), Bahamas speleothems (purple, Hoffmann et al., 2010), and various tropical coral

167   **datasets (Bard et al., 1998; Cutler et al., 2004; Durand et al., 2013; Fairbanks et al., 2005, shown in light blue, olive,**
168   **red, and green, respectively). The black lines encompass the ±1σ uncertainties of IntCal13 (Reimer et al., 2013).**

169   that have been anchored to GICC05 by matching solar variability present in all [10]Be records, and volcanic tie-

170   points (Raisbeck et al., 2017).

171   By calculating fluxes we make a first order correction for the changing snow accumulation rates between

172   stadials and interstadials and their influence on radionuclide concentrations (Wagner et al., 2001b; Johnsen et

173   al., 1995; Rasmussen et al., 2013; Finkel and Nishiizumi, 1997). The accumulation rates for each ice core are

174   based on their annual layer thickness – derived from their individual timescales – corrected for ice thinning. For

175   the Greenland ice cores this thinning function is based on a 1-D ice flow model (Dansgaard and Johnsen, 1969;

176   Johnsen et al., 1995; Johnsen et al., 2001; Seierstad et al., 2014). For the Antarctic ice cores we use the strain

177   rate derived from the Bayesian ice-core dating effort AICC12 (Veres et al., 2013). These strain rates are

178   inherently uncertain and independently derived accumulation rate estimates differ by up to 10-20% in the glacial

179   (Gkinis et al., 2014; Rasmussen et al., 2013; Guillevic et al., 2013). However, these differences are largely

180   systematic and change only on multi-millennial timescales. The shorter term changes in accumulation rates are a

181   more direct function of the timescale that determines the age-depth relationship and, thus, annual layer

182   thickness, and is very precise for increments of the core (Rasmussen et al., 2006). This is important to note, as

183   we mainly exploit production rate changes on centennial to millennial timescales for synchronization.

184   To test for additional climate influences on [10]Be or[36]Cl deposition in the ice cores, we followed the approach by

185   Adolphi and Muscheler (2016): For each ice core we calculated multiple linear regression models using $\delta^{18}O$

186   and snow accumulation rates as predictors for [10]Be ([36]Cl) fluxes and subtracted the obtained model from the

187   [10]Be ([36]Cl) data. We denote the resulting record as the "climate corrected flux" (Flux$_c$). This approach may

188   correct climate effects on [10]Be ([36]Cl) deposition insufficiently, or it may over-correct them, so it cannot be

189   assumed per se that the resulting record is more reliable than the original fluxes. Nevertheless, it provides a first

190   order sensitivity test for the ice-core records with respect to climate-related transport and depositional effects on

191   [10]Be ([36]Cl) fluxes.

192   To combine all ice-core records, we calculated their mean (denoted as "Stack", Fig. 1) using Monte-Carlo

193   bootstrapping (Efron, 1979). Using 7 ice-core records in two versions (flux and flux$_c$) yields a total number of

194   14 samples. In each iteration, 14 samples are randomly drawn (with replacement, i.e., each record can be drawn

195   multiple times), perturbed within measurement errors, and stacked. Repeating this procedure 1,000 times we

196   obtain an average relative standard deviation of 8% between the derived stacks, which is comparable to the

197   measurement uncertainty of individual measurements but larger than the expected error of the mean which

198   points to systematic differences between the records. For the period where we have data from both hemispheres

199   this standard deviation is only slightly higher (10%). Even though this is only a relatively short period (see Fig.

200   1), it contains multiple DO-events which are expressed differently in Northern and Southern Hemisphere

201   climate. Thus, this agreement can serve as indication that climate effects do not dominate the signal.

202   **3.2 Radiocarbon data**

203   For the purpose of this study we have to focus on radiocarbon records that are absolutely dated. Furthermore,

204   the length and sampling resolution of the records need to be sufficient to resolve centennial-to-millennial

205   production rate changes. The records that fulfil these criteria are shown in figure 1 and comprise ^{14}C data from

206 various U/Th dated coral records (Bard et al., 1998; Durand et al., 2013; Cutler et al., 2004; Fairbanks et al.,

207 2005), as well as ^{14}C measured in two speleothems (Southon et al., 2012; Hoffmann et al., 2010). In addition,

208 we use the ^{14}C record from Lake Suigetsu (Bronk Ramsey et al., 2012) since the U/Th dated records do not

209 directly reflect atmospheric ^{14}C but the ocean mixed layer (corals) and, in the case of speleothems, a mixture of

210 atmospheric and soil CO_2, and carbonate bedrock from above the cave. The timescale of the Lake Suigetsu

211 record is based on varve counting, corrected for long-term systematic errors by matching its ^{14}C record to the

212 ^{14}C variations in speleothems (Bronk Ramsey et al., 2012). Hence, it is not truly independently dated. However,

213 similar to ice-core layer counting, this varve count adds constraints especially on centennial timescales, so that

214 $\Delta^{14}C$ variations on these timescales should be relatively unaffected by this tuning to the speleothem ^{14}C data.

215 Thus, even though the timescale may not be independent, this record can still be used to verify the existence of

216 $\Delta^{14}C$ variations in the atmosphere seen in the mixed layer records.

217 In addition, we use the available tree-ring records back to 14,000 cal BP (calibrated before present, AD 1950) in

218 the revised version by Hogg et al. (2016)(not shown in figure 1 for clarity).

3.3 Carbon cycle modelling

220 To be able to compare ice-core and radiocarbon records directly we have to account for the effects of the carbon

221 cycle. Following earlier studies (Muscheler et al., 2004; Muscheler et al., 2008), we use a box-diffusion carbon

222 cycle model (Siegenthaler et al., 1980) to model $\Delta^{14}C$ from the ice-core radionuclide records. We assume that

223 ice-core [10]Be ([36]Cl) variations are proportional to ^{14}C production rate changes (see also following section) and

224 model $\Delta^{14}C$ anomalies from each realization of the ice-core stack, as well as the single ice-core records (Fig. 2).

225 It can be seen that the modelled $\Delta^{14}C$ records from the individual ice-core records differ in their long-term

226 trends since the carbon cycle integrates over time so that relatively small but systematic differences in the

227 radionuclide fluxes (possibly arising from uncertainties in the strain rates) have a significant effect on longer

228 time scales. However, all records show the same overall evolution of $\Delta^{14}C$. Furthermore, especially when

229 subtracting the long-term trend and isolating variations on timescales shorter than 5000 years, the agreement is

230 very high (on average within 15‰ at 1σ, Fig. 2b), which is the part of the signal that we will be exploiting in

231 our synchronization effort.

3.3.1 Production rate ratio

233 Modeling $\Delta^{14}C$ values from [10]Be measurements is based on the assumption that [10]Be and ^{14}C production rate

234 changes are proportional to each other. However, different production rate models differ in their sensitivity of

235 ^{14}C and [10]Be production rate changes to variations in the geomagnetic field (Cauquoin et al., 2014). For a given

236 geomagnetic field change, the production rate model by Masarik and Beer (2009, 1999) yields 30-50% lower

237 [10]Be production rate changes than the calculations by Poluianov et al. (2016) and Herbst et al. (2016). For ^{14}C on

238 the other hand, all models yield roughly similar amplitudes. This leads to differences in the ^{14}C/[10]Be production

239 rate ratio for a given change in the geomagnetic field. If Masarik and Beer (1999) are correct, the variations in

240 ice-core [10]Be records have to be upscaled by 30-50% to be proportional to ^{14}C production rate changes while no

241 such scaling is necessary when the other production rate models are used. In addition, the amplitudes in ^{14}C and

242 [10]Be may differ due to the presence of polar bias (see section 2). If this effect was present, then geomagnetic

243 field changes should cause bigger variations in ^{14}C than [10]Be.

244 Since the presence of a polar bias is debated and the physical reason for the differences between the production
245 rate models is unresolved, we chose an empirical approach to scale the ice-core record appropriately:
246
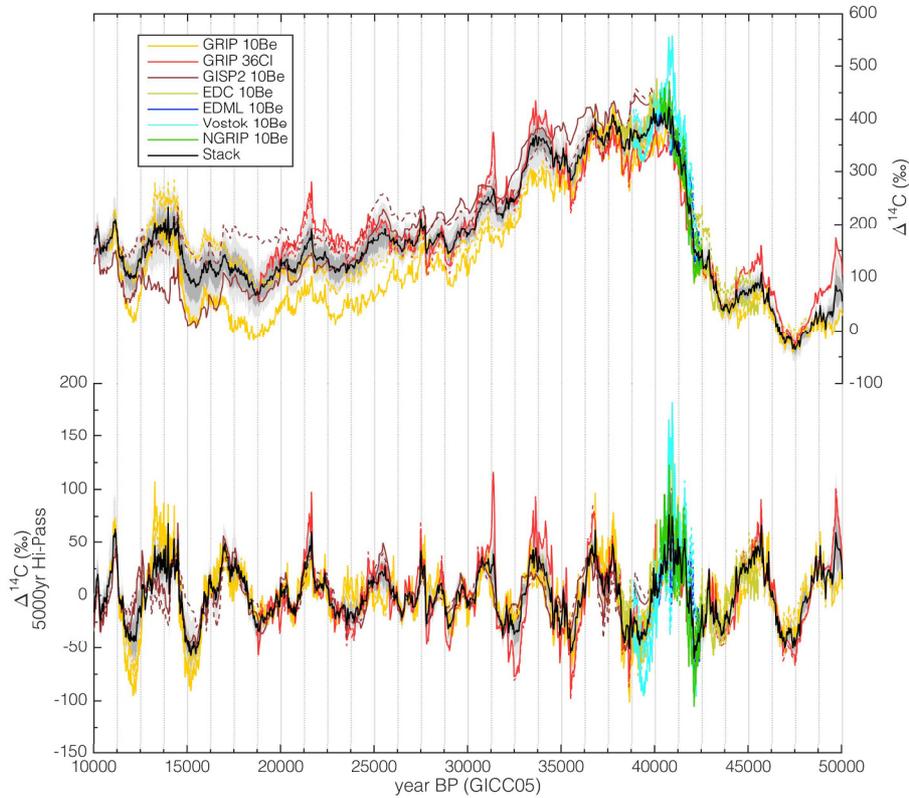
247
248 **Figure 2: Modelled Δ^{14}C anomalies from individual ice-core records (see legend, solid lines are based on radionuclide**
249 **fluxes while dashed lines are inferred from flux$_c$) and the realizations of the ice-core stack (black line shows the mean**
250 **of all realizations, dark and light grey shading encompass 68.2 and 95.4% probability ranges). The top panel shows**
251 **the unfiltered model output. The bottom panel displays the records after variations with frequencies <1/5000a^{-1} have**
252 **been subtracted (FFT-based filter).**

253 We use three geomagnetic field intensity reconstructions around the Laschamp geomagnetic field minimum (Laj
254 et al., 2004; Laj et al., 2000; Nowaczyk et al., 2013) and calculate the resulting ^{10}Be production rate changes
255 using the production rate models by Masarik and Beer (1999) and Herbst et al. (2016) (Fig. 3 a-c).
256 Subsequently, we scale the ice-core ^{10}Be record to minimize the root mean square error (RMSE) between ice-
257 core and geomagnetic field-based records (Fig. 3d). It can be seen that the RMSE reaches a minimum for a ^{10}Be
258 scaling factor of ~1 (for Masarik and Beer, 1999) and ~1.3 (for Herbst et al., 2016). This represents a fortunate
259 coincidence; irrespective of which production rate model is used, the amplitude of the ice-core ^{10}Be variations
260 has to be increased by approximately 30% to match ^{14}C. If the production rate model by Masarik and Beer is
261 used, then the amplitude of the ice-core ^{10}Be record is in agreement with geomagnetic field data, but due to the
262 higher production sensitivity of ^{14}C (see above), ^{10}Be variations have to be increased by ~30%. Similarly, if the
263 production rate model by Herbst et al. is used, then the amplitude of the ice-core ^{10}Be record is 30% smaller
264 than implied by geomagnetic field data (possibly due to a polar bias), while the sensitivity of ^{14}C and ^{10}Be is the
265 same. Again, the net effect is the ^{10}Be variations have to be scaled up by 30% for the comparison to ^{14}C.

266
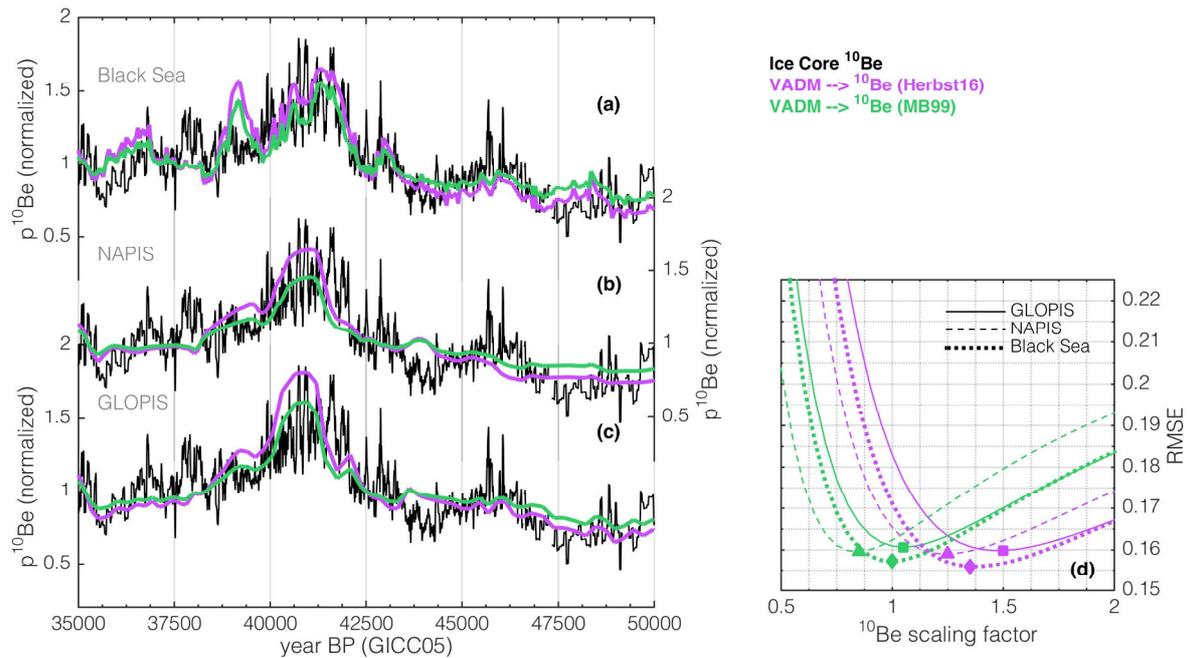
267 **Figure 3: Comparison of ice-core-based and geomagnetic-field-based reconstructions of [10]Be production rates. Panel**
268 **a-c show the ice-core stack (black) in comparison to [10]Be production rates based on geomagnetic field reconstructions**
269 **and 2 different production rate models (Herbst et al. (2016) in pink and Masarik and Beer (1999) in green). Panel a,**
270 **the Black Sea geomagnetic field record (Nowaczyk et al., 2013), Panel b, the NAPIS geomagnetic field stack (Laj et**
271 **al., 2000), and Panel c, the GLOPIS geomagnetic field stack (Laj et al., 2004). Panel d shows the RMSE between the**
272 **ice-core data and the geomagnetic-field-based records when variations in the ice-core record are scaled by different**
273 **factors (x-axis). The colours correspond to the production rate models. The line styles indicate the geomagnetic field**
274 **records (see legend) and the symbols denote the RMSE minima.**

275 **3.3.2 The state of the carbon cycle**

276 As mentioned in section 2, a quantification of transient carbon cycle changes and their influence on Δ^{14}C is

277 challenged by insufficient knowledge of inventories and processes. The contribution of single processes to Δ^{14}C

278 changes over the last glacial cycle is likely within 30‰ and, due to compensating effects, also their combination

279 is likely not bigger than 40‰ (Köhler et al., 2006). Here we use the Laschamp event to estimate the state of the

280 ocean ventilation around 40 ka BP.

281 The datasets underlying IntCal13 all show an increase of about 320‰ in Δ^{14}C into the Laschamp event (Fig. 4),

282 albeit at different absolute levels (see Fig. 1). This is ~100‰ more than the compiled IntCal13 curve itself

283 implies. This disagreement can be explained by differences in timing and absolute Δ^{14}C between the different

284 datasets leading to smoothing and dampening of Δ^{14}C variations during the construction of IntCal13. Also,

285 geomagnetic field changes yield a Δ^{14}C change more in line with the individual ^{14}C datasets than with IntCal13,

286 even when assuming a preindustrial carbon cycle.

287 To estimate the mean state of the carbon cycle during this period, we run our carbon cycle model with different

288 (constant) values of ocean diffusivity. We find that modelled and measured Δ^{14}C around the Laschamp event

289 match best in amplitude when we run the model under conditions where ocean ventilation is reduced to ~75% of

290 its preindustrial value (Fig. 4). This is in broad agreement with previous modelling experiments (Köhler et al.,

291 2006; Roth and Joos, 2013) and proxy data (Henry et al., 2016).

292 In the following, we will use this estimate for the parameterization of our model. As mentioned above, a

293 transient adjustment of carbon cycle parameters is uncertain and will hence not be attempted. Instead, we

294 ascribe an associated uncertainty to the modelled Δ^{14}C based on the carbon cycle sensitivity experiments by

Köhler et al. (2006). Furthermore, it should be noted, that by only using (filtered) Δ^{14}C anomalies as synchronization targets, we i) avoid systematic carbon cycle influences on Δ^{14}C levels, and ii) minimize transient carbon cycle related changes in Δ^{14}C (Adolphi and Muscheler, 2016).
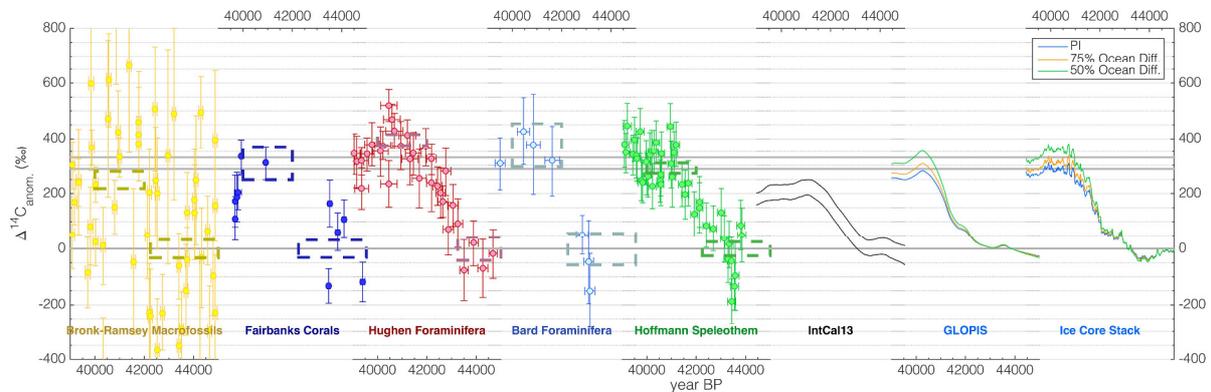
Figure 4: The Laschamp event in measured and modelled Δ^{14}C. The 6 panels to the left show Δ^{14}C anomalies from macrofossils from Lake Suigetsu (yellow, Bronk Ramsey et al., 2012), tropical corals (blue, Fairbanks et al., 2005), foraminifera from Cariaco Basin sediments (red, Hughen et al., 2006), foraminifera from Iberian Margin sediments (light blue, Bard et al., 2013), Bahamas speleothems (green, Hoffmann et al., 2010), and IntCal13 (black, Reimer et al., 2013). All data are shown as anomalies to their error-weighted mean prior to the Laschamp event. i.e., the Δ^{14}C increase. The dashed boxes encompass the time periods and Δ^{14}C uncertainties (error of the error weighted mean) used for the definition of the pre-and post-Laschamp event levels. The two panels on the right show modelled Δ^{14}C using the GLOPIS (Laj et al., 2004) geomagnetic field record as well as the ice-core stack as production rate inputs. The different coloured lines reflect different carbon cycle scenarios (see legend, PI denotes pre-industrial). The conversion of geomagnetic field intensity to ^{14}C production rate is based on the production rate model by Herbst et al. (2016). Note, that the amplitude of the ^{10}Be variations have been increased by 30% as discussed in section 3.3.1.

3.4 Synchronization – effects of the carbon cycle and the archive

The synchronization method follows Adolphi and Muscheler (2016) and is outlined and tested in detail therein. In brief, sections of modelled (ice-core based) Δ^{14}C anomalies are compared to the measured Δ^{14}C. For our analysis we employ high-frequency changes in Δ^{14}C since carbon cycle changes have only limited effects on atmospheric Δ^{14}C on shorter time scales (Adolphi and Muscheler (2016). Similarly, as shown in figure 2, the agreement of the different ice-core records is better on shorter timescales. In this study, we employ two types of high pass filtering: a FFT-based high-pass filter and simple linear detrending. The choice of filter is based on the data sampling resolution. For the highly resolved tree-ring data we use a 1000 year high-pass FFT filter, while the lower resolved and more unevenly sampled coral/speleothem/macrofossil data is filtered by linear detrending to avoid the interpolation to equidistant resolution required for FFT analysis. Similarly, the high sampling resolution of the tree-ring data allows us to compare the data in 2,000 year windows, while we increase the window length to 4,000 and 5,000 years for the lower resolved data prior to 14ka BP. The exact frequencies and window lengths are also given in the results section. Using the same statistics as for radiocarbon wiggle-match dating (Bronk Ramsey et al., 2001), we then infer a probability density function (PDF) for the timescale difference between the modelled and measured Δ^{14}C records. For details of the statistics of this methodology we refer the reader to Adolphi and Muscheler (2016). Here we focus instead on additional uncertainties that arise when comparing modelled atmospheric Δ^{14}C to ^{14}C records from the ocean mixed layer (corals) or speleothems.

329   $\Delta^{14}C$ variations in the atmosphere are dampened and delayed compared to the causal production rate changes.

330   Both factors, attenuation and delay, depend on the frequency of the production rate change (Roth and Joos,

331   2013; Siegenthaler et al., 1980). The dampening is largest at high frequencies and decreases with longer periods.

332   On the other hand, the apparent peak-to-peak delay between sinusoidal production rate changes and the resulting

333   $\Delta^{14}C$ change is increasing with increasing wavelengths. Similar effects occur when comparing atmospheric and

334   oceanic $\Delta^{14}C$ changes to each other: the ocean reacts to atmospheric $\Delta^{14}C$ changes with a delayed and dampened

335   response that is wavelength dependent. Hence, we need to take these factors into account when comparing a

336   modelled atmospheric $\Delta^{14}C$ record to mixed layer marine records. However, the frequency dependence of the

337   attenuation and delay makes it difficult to explicitly correct for this since atmospheric $\Delta^{14}C$ changes vary on

338   different time scales simultaneously. Furthermore, the coral records vary in their sampling frequency and often

339   it is not precisely known over how much time an individual ^{14}C sample integrates.

340   Figure 5 shows a sensitivity test regarding these effects. We modelled $\Delta^{14}C$ from the ice-core stack around the

341   Laschamp event and compared the atmospheric $\Delta^{14}C$ to the mixed layer $\Delta^{14}C$ in the model. To simulate the

342   effect of varying averaging effects of the coral samples, we low-pass filtered the mixed layer signal with

343   increasing cut-off wavelengths. For each filter, we then inferred the apparent delay between the mixed layer

344   (i.e., the "coral") and the atmosphere. In doing so we infer that even though the signal is dominated by a long

345   lasting $\Delta^{14}C$ increase, the inferred delay is small (~30 years) as long as the coral samples do not integrate over

346   long times. Only when assuming that each coral sample averages over more than 1,000 years we infer delays of

347   about 120 years. Nevertheless, this experiment also shows that within reasonable bounds of averaging, the delay

348   of mixed layer to atmospheric signal is limited

349
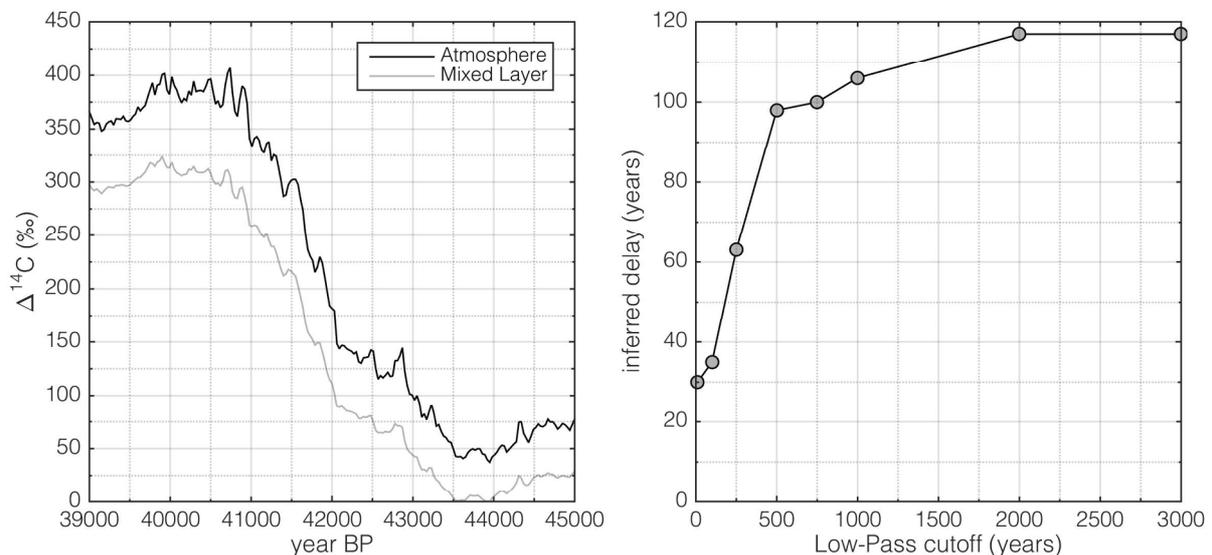
350   **Figure 5: The delay between $\Delta^{14}C$ in the atmosphere and ocean mixed layer. The left panel shows modelled $\Delta^{14}C$**
351   **from the ice-core stack around the Laschamp event. The modelled atmospheric $\Delta^{14}C$ is shown in black while ocean**
352   **mixed layer is shown in grey. They right hand panel shows the inferred delay from our synchronization method when**
353   **comparing the atmospheric to the mixed layer signal for different low-pass filters of the mixed layer signal (x-axis).**

354

355   The speleothem $\Delta^{14}C$ reacts differently than the ocean mixed layer. The so-called dead carbon fraction (DCF) of

356   a speleothem consists of two main contributors: i) respired soil organic matter that is older (in ^{14}C years) than

357   the atmospheric ^{14}C signal, and ii) carbonate bedrock that contains no ^{14}C. Applying the model of Genty and

Massault (1999), we model speleothem $\Delta^{14}C$ using different assumptions on the age of the respired soil organic matter and fraction of carbonate bedrock in drip water CO_2. We do this for 2 examples: i) a speleothem with an apparent DCF (i.e., offset from the atmosphere) of 5.8‰ (resembling the Hulu Cave speleothem record by Southon et al., 2012) and ii) a speleothem with an apparent DCF of 25.7‰ (resembling the Bahamas speleothem by Hoffmann et al., 2010). By assuming different ages of the soil respired carbon ($\tau = 10 - 400$ years, see Fig. 6), we adjust the fraction of ^{14}C-free CO_2 so that the apparent DCF for each speleothem is matched. The age of the soil respired carbon is defined following Genty and Massault (1999): if, for example, $\tau = 100$ years, then the activity of the soil respired CO_2 is the mean of the atmospheric activity over the past 100 years prior to sampling (also accounting for decay within these 100 years). For simplicity we assume a uniform age distribution for the soil respired carbon. Subsequently, we compare the modelled speleothem $\Delta^{14}C$ to the original atmospheric input using our synchronization method and plot the inferred delay (Fig. 6, right panel). From this experiment it can be seen that the controlling factor on the inferred delay is the age of the soil respired matter that acts as an integrator (low-pass filter) of the atmospheric ^{14}C signal. The fraction of ^{14}C-free carbonate has no influence on the lag between $\Delta^{14}C$ changes in the atmosphere and the speleothem, but only dampens the amplitude of the corresponding change. Realistic ages of soil respired carbon differ from region to region but even though some slow cycling fractions of soil organic matter may be up to several thousand years old (Trumbore, 2000), the major contributors to soil CO_2 are considerably younger and in the order of decades (Genty et al., 2001; Fohlmeister et al., 2011).

From these experiments we conclude that our systematic matching uncertainties to coral and speleothem records are probably below 100 years. We note that this uncertainty is asymmetric since the ocean/speleothem signal cannot lead the atmosphere and so the offset is unidirectional.
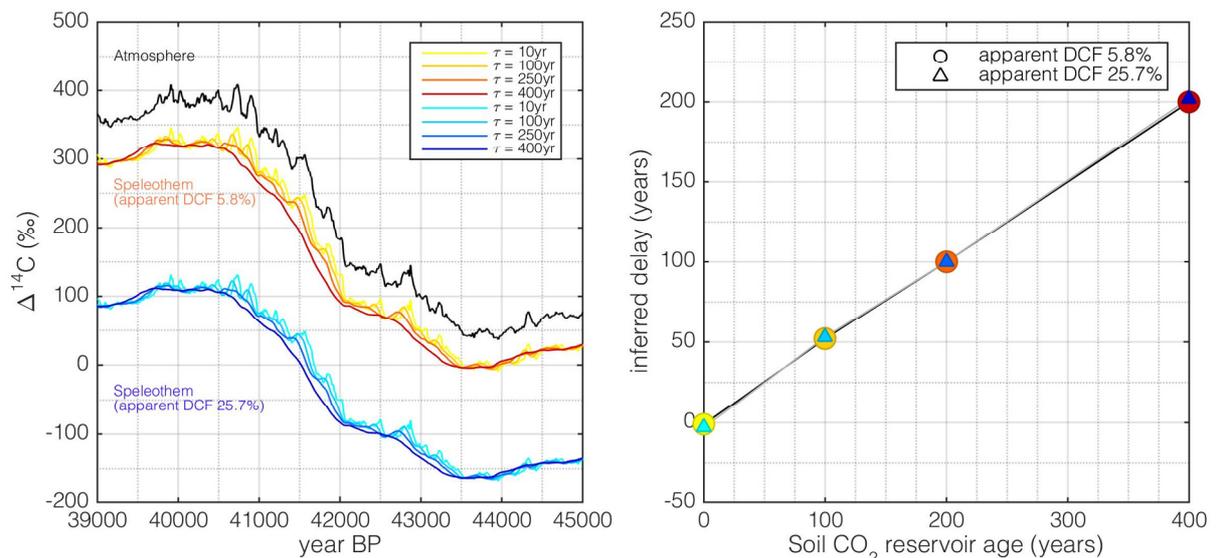
Figure 6: Effect of varying ages of soil respired CO_2 and fractions of CO_2 from ^{14}C-dead carbonate on the $\Delta^{14}C$ in speleothems. The left panel shows atmospheric modelled $\Delta^{14}C$ from the ^{10}Be stack (black) and two modelled speleothem scenarios with a net DCF of 5.8‰ (warm colours) and 25.7‰ (cold colours). For each speleothem, a number of different ages for the respired soil organic matter have been assumed (see legend) and the input of ^{14}C-free CO_2 from carbonate has been adjusted to obtain the correct apparent DCF value between 39-40.5 ka BP. The right hand panel shows the inferred delay when we apply our synchronization method to match the atmospheric $\Delta^{14}C$ to the speleothem record.

3.5 Change-point detection in climate records

To test the synchroneity of rapid climate changes, we compare the timing of DO-events seen in Greenland ice cores (Andersen et al., 2004), to a number of well-known U/Th dated speleothems that show DO-type variability from Hulu Cave (Cheng et al., 2016), Sofular Cave (Fleitmann et al., 2009), El Condor, and Cueva del Diamante (both Cheng et al., 2013b).

We use a probabilistic model to detect the onset, mid-point, and end of the rapid climate transitions in each individual record. The employed model describes the abrupt changes as a linear transition between two constant states. Any variability due to the long-term fluctuations of the climate records around the transition model is described by an AR(1) process that is estimated in conjunction with the transition model. The model is independently fitted to windows of data on their individual timescales (Table 1 & Fig. 13) around the rapid transitions. Inference was performed using Markov Chain Monte Carl sampling (MCMC) to obtain PDFs of the timing of the onset, the length, and the amplitude of each transition in each record. Using these PDFs we can calculate delays of the onset, mid-point and end of the climate transitions between different records, propagating the respective uncertainties of the parameters. For each record, only events that are well expressed and measured in high resolution have been fitted. The approach and inference procedure are described in more detail in Erhardt et al. (submitted).

Table 1. Change-point detection window for each record. For each investigated climate event and record, the change-point detection algorithm has been applied between t1 and t2. The windows have been defined visually, ensuring a sufficient amount of data prior to and after the transition. For each record, only events that are well expressed in the climate proxy records at high resolution have been investigated. For the ice-core record t1 and t2 typically encompass 500 years prior to and after the nominal transition ages by Rasmussen et al. (2014a). The exact values have been adjusted to exclude overlap with other transitions where necessary (Erhardt et al. in prep).

Event	GICC05 (yr BP)	MCE	Hulu d18O t1	Hulu d18O t2	Sofular d18O t1	Sofular d18O t2	Sofular d13C t1	Sofular d13C t2	ElCondor d18O t1	ElCondor d18O t2	Diamante d18O t1	Diamante d18O t2
Holocene	11653	99	12453	10503	12703	10703	12703	11003	12453	11203	13403	11203
GI-1e	14642	186	15442	13942	15442	13942	15442	13942	15442	14192	16392	14192
GS-3 Dust Peak	24130	645	25380	24080	-	-	-	-	-	-	25780	24630
GI-3	27730	832	28580	27680	28780	27880	28780	27780	-	-	29030	28080
GI-4	28850	898	30100	28900	30150	29400	30150	29200	29900	29000	30100	29100
GI-5.1	30790	1008	31540	30790	-	-	-	-	31590	30740	32040	30840
GI-5.2	32450	1132	33300	32200	33100	32400	33300	32200	33250	32000	33050	32450
GI-6	33690	1195	34590	33640	34740	33690	34990	33540	34240	33490	-	-
GI-7c	35430	1321	36680	34980	36380	35480	36380	35230	36230	34880	36480	34980
GI-8c	38170	1449	39420	37420	39420	37220	39120	37220	39220	37220	-	-
GI-9	40110	1580	40860	40060	40960	39960	41160	39960	-	-	-	-
GI-10	41410	1633	42110	41060	42460	41590	42460	41460	42210	40960	-	-
GI-11	43290	1736	44240	42940	44840	43540	-	-	44040	42440	-	-

4 Time scale differences between GICC05 and the U/Th timescale

In the following sections we will show the synchronization results for different time windows. We focus our analysis on three distinct windows: 10-14 ka BP, 18-25 ka BP and 39-45 ka BP. The youngest window is defined by the presence of high-resolution tree-ring data for ^{14}C back to 14 ka BP. Going further back in time it becomes increasingly challenging to unequivocally identify common structures in the various Δ^{14}C records that are suitable for synchronization because the resolution of the individual records decreases back in time while their differences to each other are growing steadily (see Fig. 1i). Hence, we focus on the well-known Laschamp

418   event around 41 ka BP, and the period between 18-25kaBP, i.e., preceding the major carbon cycle changes

419   associated with the deglaciation. We omit the period between 25-39 ka BP. As discussed in Reimer et al. (2013)

420   and seen in figure 1i there is substantial disagreement between the datasets underlying IntCal13 at that time that

421   are impossible to reconcile within their respective age and/or ^{14}C uncertainties. Hence, also any structure in the

422   Δ^{14}C records may be unreliable and thus, lead to erroneous synchronization results.

4.1 10,000 – 14,000 years BP

424   In the 10-14 ka BP interval, we synchronize the ice-core stack to high-resolution tree-ring and speleothem Δ^{14}C

425   data (Fig. 7). The high sampling resolution of the ^{14}C records allows us to focus on centennial-to-millennial

426   Δ^{14}C changes (<1000 years) where carbon cycle influences on Δ^{14}C can be expected to be small (Adolphi and

427   Muscheler, 2016). In concordance with earlier studies (Muscheler et al., 2014a) we find that GICC05 is ~65

428   years older than the tree-ring timescale at the onset of the Holocene, but that this offset vanishes over the course

429   of the Younger Dryas interval.

430   While Muscheler et al. (2014a) argued that this changing offset may be in part due to errors in the timescale of

431   the floating Late Glacial Pines, we can now support this change in the timescale-difference through the U/Th

432   dated speleothems: The synchronization of the ice-core stack to the H82 speleothem from Hulu Cave (Southon

433   et al., 2012) leads to fully consistent results as inferred from the tree-rings. This indicates that the most likely

434   explanation is an ice-core layer counting bias, i.e. that the GICC05 time scale suggests too old ages at the onset

435   of the Holocene, but is accurate within a few decades during GI-1.
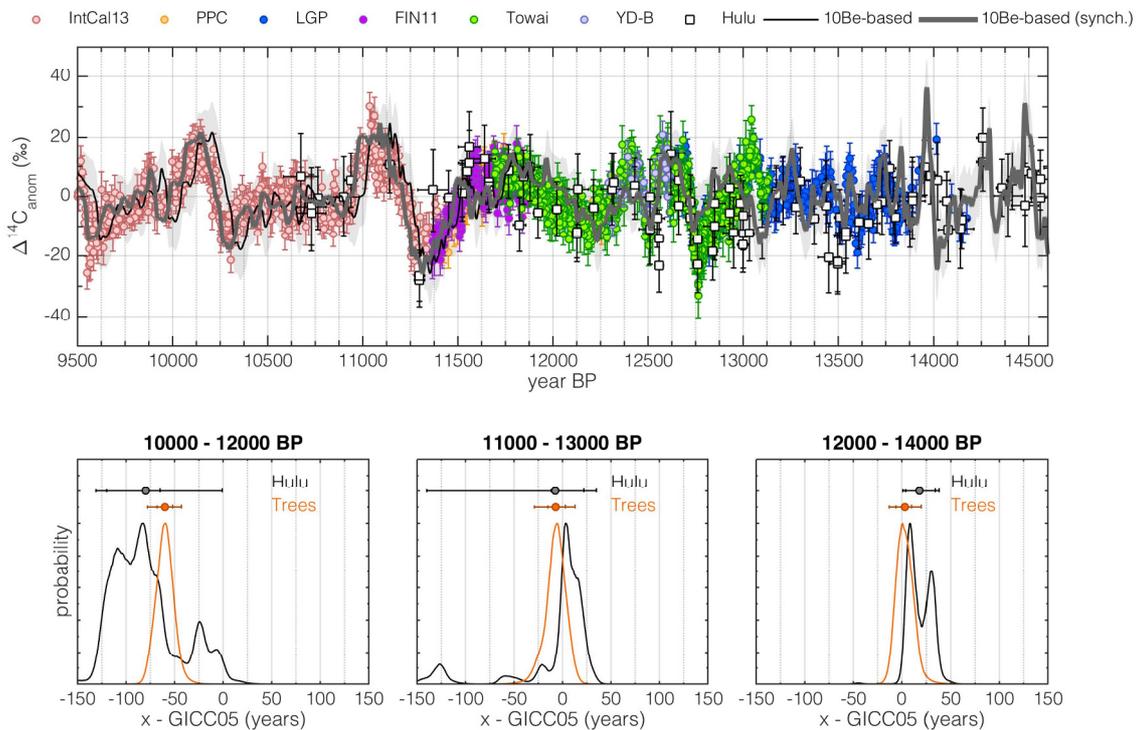
436

437 **Figure 7: Synchronization of GICC05 to tree-ring and Hulu Cave records during the last deglaciation. Top panel:**
438 **Ice-core based modelled Δ^{14}C anomalies on the original GICC05 timescale (thin black line, light grey shading**
439 **encompasses the ±10‰ uncertainty (±1σ) of the modelled Δ^{14}C, based on the carbon-cycle sensitivity experiments by**
440 **Adolphi & Muscheler (2016)) and synchronized timescale (bold grey line). Tree-ring data underlying IntCal13 are**
441 **shown in pink. Revised Northern Hemisphere tree-ring data according to Hogg et al. (2016) are shown in orange**
442 **(Preboreal Pines), dark blue (Late Glacial Pine) and light blue (Younger Dryas-B chronology). New kauri Δ^{14}C data**
443 **by Hogg et al. (2016) is shown in purple (FIN11) and green (Towai). Hulu Cave H82 Δ^{14}C data are shown as white**

Interestingly, we do not observe any significant differences between the results stemming from tree-rings and the speleothem records. As shown in section 3.4, we could expect a delay in the speleothem Δ^{14}C compared to the atmosphere if the respired soil organic carbon contribution to the soil CO_2 was very old. This would result in GICC05 appearing older in comparison to the speleothem than relative to the tree rings. The lack of this delay implies that the majority of the respired soil organic carbon at Hulu Cave must be younger than ~100 years (see Fig. 6). This is supported by the fact that the centennial Δ^{14}C variations in the tree-ring and speleothem data have the same amplitude (Fig. 7). If old organic carbon significantly contributed to the soil CO_2, we would instead expect to see a stronger smoothing of short-term Δ^{14}C variations.

4.2 18,000 – 25,000 years BP

Due to the irregular and lower sampling resolution of the ^{14}C records beyond 15,000 cal BP, we chose to linearly detrend each data set (instead of band-pass filtering) to remove offsets between the different ^{14}C datasets (see figure 1i) and highlight common variability. Furthermore, we have to increase the length of the comparison data windows to 4,000 years to ensure sufficient structure in the ^{14}C sequences entering the comparison. Each window is detrended separately in the analysis to isolate short-term Δ^{14}C variability. We note however, that detrending each ^{14}C dataset over the entire timeframe (18-25 ka BP) instead does not alter the results significantly. Compared to the high-frequency Δ^{14}C changes studied between 10-14 ka BP, the longer-term variations used for synchronization here may have been increasingly affected by carbon-cycle changes. To account for this, we increase the uncertainty estimate of the modelled Δ^{14}C changes to ±30‰ (±1σ), which is sufficiently large to account for estimated carbon-cycle-driven Δ^{14}C changes from modelling experiments during the entire glacial (Köhler et al., 2006). We note that this is a conservative estimate, given that during this period neither modelling (Köhler et al., 2006; Muscheler et al., 2004), nor data (Eggleston et al., 2016) suggest large carbon-cycle changes.

471
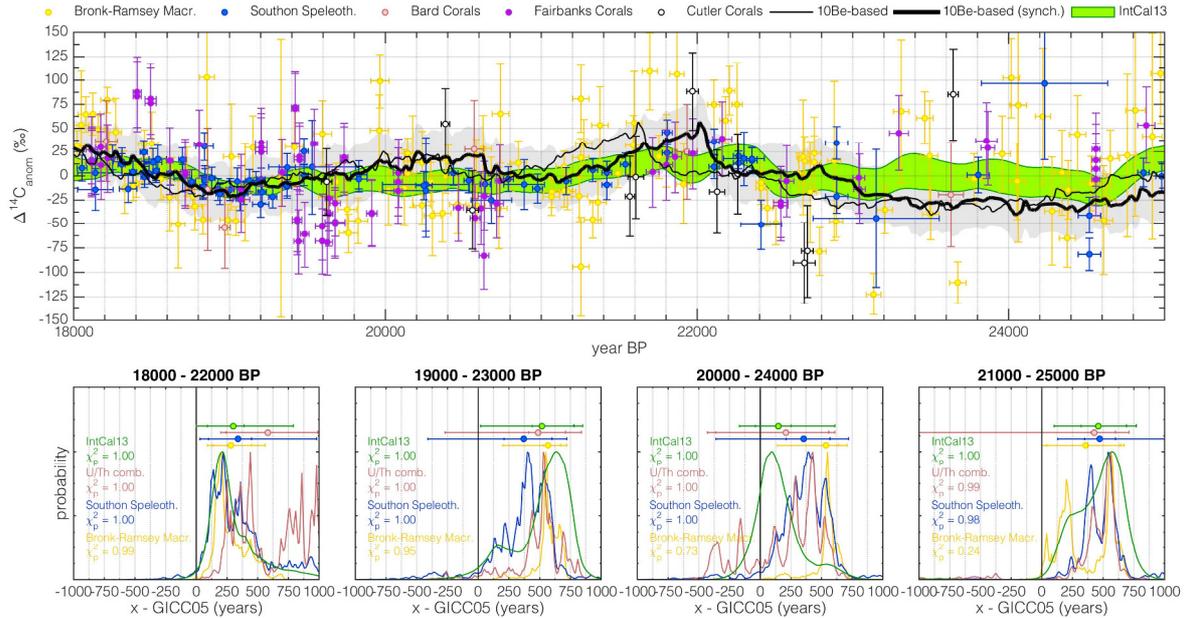
Figure 8: Synchronization results between 18,000 and 25,000 years BP. Top panel: The thin black line shows the modelled $\Delta^{14}C$ curve based on the ice-core stack on its original timescale. The bold black line and grey shading show the synchronized ice-core record including assumed ±1σ uncertainties of ±30‰. The different coloured symbols indicate various ^{14}C datasets underlying IntCal13, which is shown as the green envelope. Lower panels: Each panel shows PDFs of the inferred timescale difference between the ice-core stack and IntCal13 (green), a combination of all U/Th-dated records (speleothems/corals, pink), the H82 speleothem (blue), and Lake Suigetsu (yellow). Symbols of similar colour show the inferred mean and 68.2% and 95.4% confidence intervals. Colour-coded text indicates χ^2 probabilities for the goodness of fit between modelled and measured $\Delta^{14}C$ curves after synchronization. Small (e.g., <0.1) values would indicate significant disagreement. Note that all χ^2 probabilities are relatively high, indicating that our uncertainty estimate for the modelled $\Delta^{14}C$ is very conservative. Each of the lower panels refers to a specific subsection of the data indicated at the top of each panel.

It can be seen in figure 8 that it is challenging to infer robust co-variability in multiple ^{14}C records. However, the millennial evolution of $\Delta^{14}C$ does show common changes in the 18-25 ka BP interval. Synchronizing the ice-core stack to data from i) Hulu Cave H82 speleothem, ii) Lake Suigetsu macrofossils, iii) the IntCal13 stack or iv) a combination of all U/Th dated records (speleothems/corals) leads to consistent results within uncertainties for each choice of time windows: all records imply that GICC05 shows younger ages compared to the ^{14}C records around this time.

The most significant structure that is present in all measured and modelled ^{14}C records during this time is the centennial $\Delta^{14}C$ increase around 22.1kaBP (see Fig. 9). Comparing the ice-core stack to $\Delta^{14}C$ between 21-23kaBP indicates an offset of ~550 years between GICC05 and the U/Th timescale around this time (GICC05 being younger). To account for the potential delay of coral and speleothem $\Delta^{14}C$ compared to the atmosphere, we also modelled the mixed layer $\Delta^{14}C$ signal from the ice-core stack and synchronized this signal to the measured ^{14}C data (Fig. 9). As discussed in section 3.4, we find very little difference in the inferred timing since the $\Delta^{14}C$ variation is relatively rapid (centuries). Comparing the $\Delta^{14}C$ anomalies to geomagnetic field data shows that a small part of the longer-term development of this structure is probably driven by geomagnetic field changes. The amplitude (~50‰) and short duration (centuries) of the $\Delta^{14}C$ increase, however, suggest that this change is mainly driven by a series of strong solar minima, comparable to the Grand Solar Minimum period around the onset of the Younger Dryas (Muscheler et al., 2008). We used this tie-point (figure 9) in the final

  synchronization as it is the best-defined feature in this time interval, and consistent within error with the
  estimates shown in figure 8.
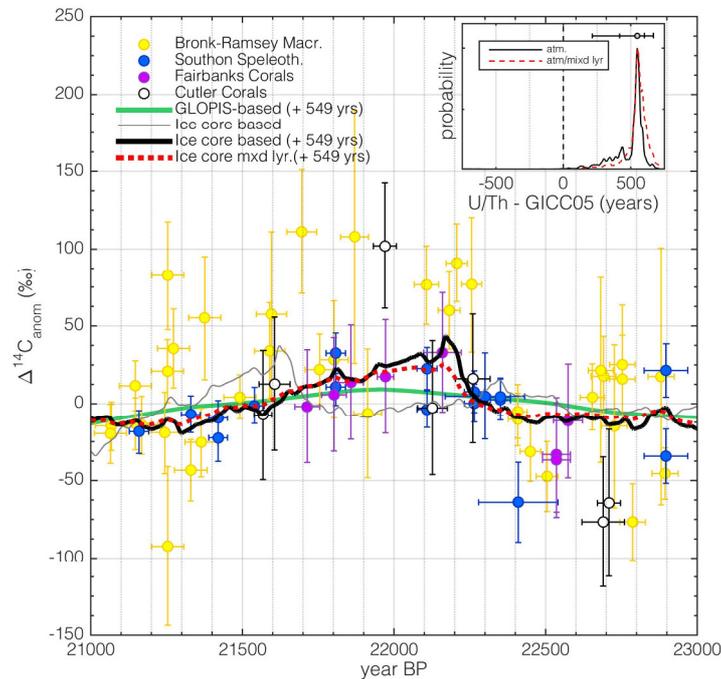
Figure 9: Close-up of measured and modelled $\Delta^{14}C$ anomalies between 21 and 23 ka BP. The thin grey line shows modelled atmospheric $\Delta^{14}C$ from the ice-core stack on the GICC05 time scale. The bold black and dashed red lines show the modelled atmospheric and ocean mixed layer $\Delta^{14}C$ curves after synchronization to the ^{14}C records (yellow: Lake Suigetsu; blue: Hulu Cave; purple and white: corals). The inset panel shows the PDF of the inferred timescale difference between GICC05 and the combination of all ^{14}C records. The black line is based on using only the modelled atmospheric $\Delta^{14}C$. The red dashed line is based on comparing coral and speleothem data to the modelled mixed-layer $\Delta^{14}C$, and Lake Suigetsu data to modelled atmospheric $\Delta^{14}C$. The green line shows modelled $\Delta^{14}C$ based on geomagnetic field changes.

4.3 39,000 – 45,000 years BP

Our oldest tie-point is the previously discussed Laschamp event around 41 ka BP. The only independently and absolutely dated ^{14}C record around this time that has a sufficient sampling resolution is the Bahamas speleothem by Hoffmann et al. (2010). While offset in absolute $\Delta^{14}C$ (see Fig. 1), the U/Th-dated coral data supports the amplitude and timing of the $\Delta^{14}C$ increase seen in the speleothem even though precise synchronization is hampered by the low sampling resolution of the corals. The Lake Suigetsu record is characterized by large uncertainties and scatter around this time. As discussed in section 3.3.2, IntCal13 is smoothed around Laschamp, having a smaller amplitude and a less sharp rise in $\Delta^{14}C$. For this tie-point, we merely remove the error-weighted mean between 39-45 ka BP from each dataset, since detrending would remove the largest part of the signal. Hence, there are large $\Delta^{14}C$ modelling uncertainties associated with unknown carbon-cycle changes, and we assume a Gaussian $\pm 1\sigma$ error of 50‰, which we consider conservative since sensitivity experiments imply that the impact of carbon cycle changes on $\Delta^{14}C$ was likely below 40‰ (Köhler et al., 2006).
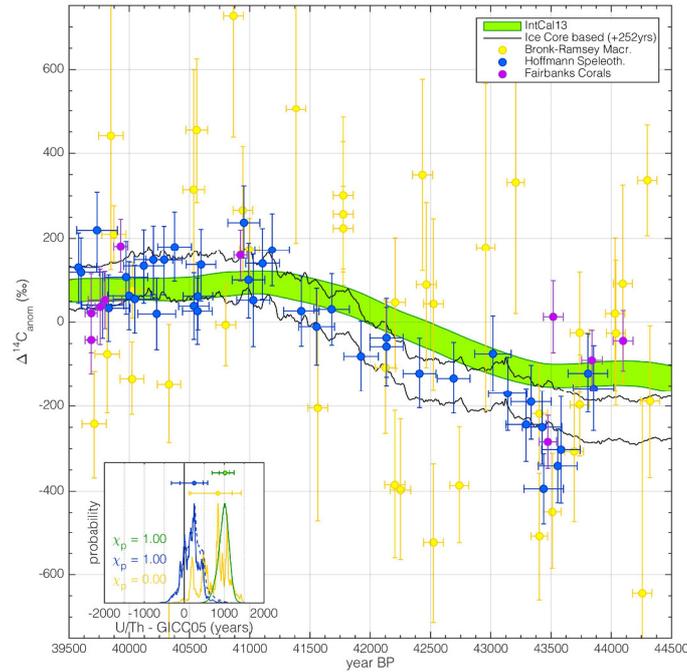
Figure 10. Synchronization of ¹⁰Be and ¹⁴C around the Laschamp event. The black lines encompass the modelled Δ¹⁴C anomalies (±1σ) from the ice-core data shifted by +252 yrs (68.2% confidence interval = -103 to 477 yrs) according to their best fit to the speleothem ¹⁴C data. The green patch shows the ±1σ envelope of IntCal13. The blue and purple symbols show Δ¹⁴C from Bahamas speleothem, and corals, respectively. The yellow symbols show Δ¹⁴C anomalies based on Lake Suigetsu macrofossils. All datasets have been centred to 0‰ by subtracting the error-weighted mean of each dataset. The inset shows the PDF of the inferred age differences between the ice-core data and IntCal13 (green), Lake Suigetsu (yellow) and the Bahamas speleothem (blue). The dashed blue line corresponds to age differences from the modelled mixed layer Δ¹⁴C and the Bahamas speleothem.

Synchronizing the ice-core stack to the speleothem, Lake Suigetsu, and IntCal13 data yields significantly different results. We infer that GICC05 produces ages about 250 years younger than the U/Th dated speleothem data (Fig. 10). The IntCal13 record however, implies a larger difference of ~1,000 years. Using Lake Suigetsu data, on the other hand, leads to multiple probability peaks of which two are in agreement with the speleothem, and one with the IntCal13 record. The large scatter of the Lake Suigetsu data however, leads to poor statistics (low χ^2 probabilities). Furthermore, the Lake Suigetsu timescale is only constrained by varve counting back to 39 ka BP and based on extrapolation for older sections (Bronk Ramsey et al., 2012) and hence, provides less precise constraints on the timing of the Δ¹⁴C increase.

To test which of these links is the most likely we turn to independent radiometric ages of the Laschamp excursion. Pooled Ar-Ar, K-Ar, and U/Th ages on lava flows place the period of (nearly) reversed field direction at 40,700 ± 950 yr BP (Singer et al., 2009), or 41,300 ± 600 yr BP (Laj et al., 2014). In addition, a North American speleothem provides a U/Th-dated transient evolution of the geomagnetic field (Lascu et al., 2016), with the lowest intensities occurring at 41,100 ± 350 yr BP. Comparing the ice-core ¹⁰Be stack to these data clearly shows that all of these records rule out the +1,000 year time shift implied by IntCal13, as it would induce a significant disagreement between radiometrically dated magnetic field records and the dating of the ¹⁰Be peak in the ice cores (Fig. 11). We hence argue that the 252 yr offset inferred from the comparison to the Bahamas speleothem is the most likely estimate of the timescale difference between GICC05 and the U/Th timescale around this time. Similar as before, assuming that the speleothem represents a mixed-layer signal instead of

553 direct atmospheric Δ^{14}C does not significantly affect the inferred timescale differences (see Fig. 10 inset, blue

554 dashed line).

555
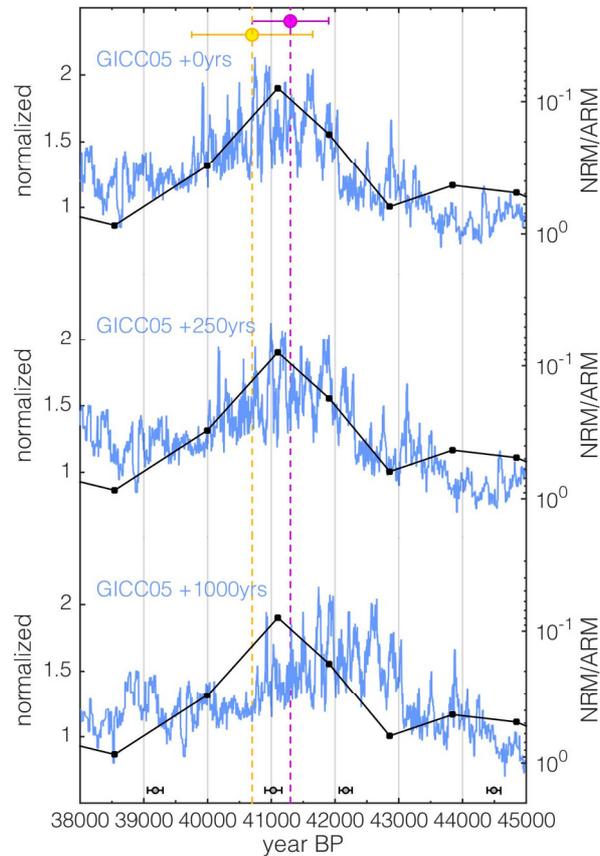
556
557 **Figure 11: Comparison of the ice-core stack (blue) to Ar-Ar dates of the Laschamp excursion (yellow: Singer et al.**
558 **2009, pink: Laj et al. 2014), and relative geomagnetic field intensity (black, NRM/ARM, reversed y-axis) from a**
559 **U/Th-dated speleothem (Lascu et al., 2016). The individual speleothem U/Th dates are shown on the bottom of the**
560 **figure with their ±2σ uncertainties. Each panel shows a different shift of GICC05 according to the results from figure**
561 **10.**

562

4.4 Transfer Function

564 To construct a continuous transfer function between GICC05 and the U/Th timescale we apply a Monte Carlo

565 approach. Each iterations consists of i) randomly sampling the PDFs at each tie-point and ii) interpolating in

566 between the tie-points using an AR-process that is constrained by the GICC05 maximum counting error (mce).

567 We use the tie-points shown in figure 7, 9, and 10, i.e., three tie-points between ice cores and tree-rings during

568 the deglaciation, one tie-point between ice cores and the combination of Corals, Speleothems and Lake Suigetsu

569 during the LGM, and one tie-point between ice cores and the Bahamas speleothem around the Laschamp event.

570 For the interpolation, we use the time derivative of the mce (i.e., its growth rate) as an incremental error

571 estimate. During periods when the growth rate is > 0 GICC05 may be stretched (compressed), while a growth

572 rate of 0 does not allow this, independent of what the absolute mce is at that time. By multiplying this growth

573 rate with a random realization of an AR-process, we simulate how much of that uncertainty has been realized in

574 each iteration of the Monte Carlo simulation. Subsequently integrating over the resulting timeseries of simulated

575 miscounts, we obtain again an absolute error estimate, i.e., one possible realization of the mce. In each iteration,
576 this realisation is then anchored at the sampled tie-points (step i) by linearly correcting the offset between the
577 sampled tie-points and the simulated counting error. Hence, this procedure provides us with a correlated
578 interpolation uncertainty over time, taking into account some of the constraints provided by the ice core
579 timescale itself, but giving priority to our inferred tie-points. We note that this treatment of the mce as an AR-
580 process leads to larger interpolation errors compared to assuming a white noise model, which would lead to very
581 small uncertainties that average out over long time (see also discussion in Rasmussen et al., 2006). Furthermore,
582 we treat the mce as $\pm1\sigma$ instead of $\pm2\sigma$ as proposed by Andersen et al. (2006) which additionally increases our
583 interpolation error. We stress that this procedure does not aim to provide a realistic model of the ice-core layer-
584 counting process and its uncertainty which is clearly more complex (see Andersen et al., 2006; Rasmussen et al.,
585 2006), nor should it be interpreted such that the mce was a 1σ uncertainty. However, our approach allows us to
586 infer a conservative estimate of the interpolation uncertainty while at the same time it takes advantage of the fact
587 that GICC05 is a layer counted timescale and hence, cannot be stretched/compressed outside realistic bounds.
588 This procedure was repeated 300,000 times which was found sufficient to obtain a stationary solution, leading to
589 300,000 possible timescale transfer functions.
590 Figure 12 shows the resulting mean transfer function along with its confidence intervals. Firstly, it can be seen
591 that all tie-points fall into the uncertainty envelope of GICC05. The implied change in the timescale difference
592 between the youngest two tie-points (i.e., over the course of GS-1), and between 13,000 and 22,000 years BP is
593 slightly larger than allowed by the mce, albeit the latter is consistent within the uncertainties of the tie-point at
594 22,000 years BP. We can see that the use of the mce to determine the interpolation error leads to small
595 uncertainties wherever the change in the timescale difference is large (e.g. over the 13,000 – 22,000 years BP
596 interval): Stretching GICC05 by as much as the counting error allows, requires that every uncertain layer has in
597 fact been a real annual layer, leaving little room for additional error. Between 22,000 and 42,000 years BP, the
598 interpolation uncertainties are determined by the mce and thus, grow/shrink at a rate determined by the mce.
599 Our results are in very good agreement with the results by Turney et al. (2016) around Heinrich 3. In this study,
600 a kauri-tree ^{14}C sequence was calibrated onto Lake Suigetsu ^{14}C and also matched on GICC05 via ^{10}Be. The
601 difference of the inferred ages (i.e., kauri on Suigetsu vs. Kauri on GICC05) matches with our proposed transfer
602 function (red star in Fig. 12).
603 Figure 12 also shows the inferred offset between the ^{40}Ar/^{39}Ar-age of the Campanian Ignimbrite (Giaccio et al.,
604 2017) and a tentatively attributed SO_4-spike in the GISP2 ice core (Fedele et al., 2007). Even though it
605 obviously requires a well-characterized tephra find in the ice cores to ensure that the SO_4-peak is indeed
606 associated with the Campanian Ignimbrite, at least from a chronological point of view, our transfer function
607 does not preclude this link. However, no matching shards were identified in this period (Bourne et al., 2013).
608

609
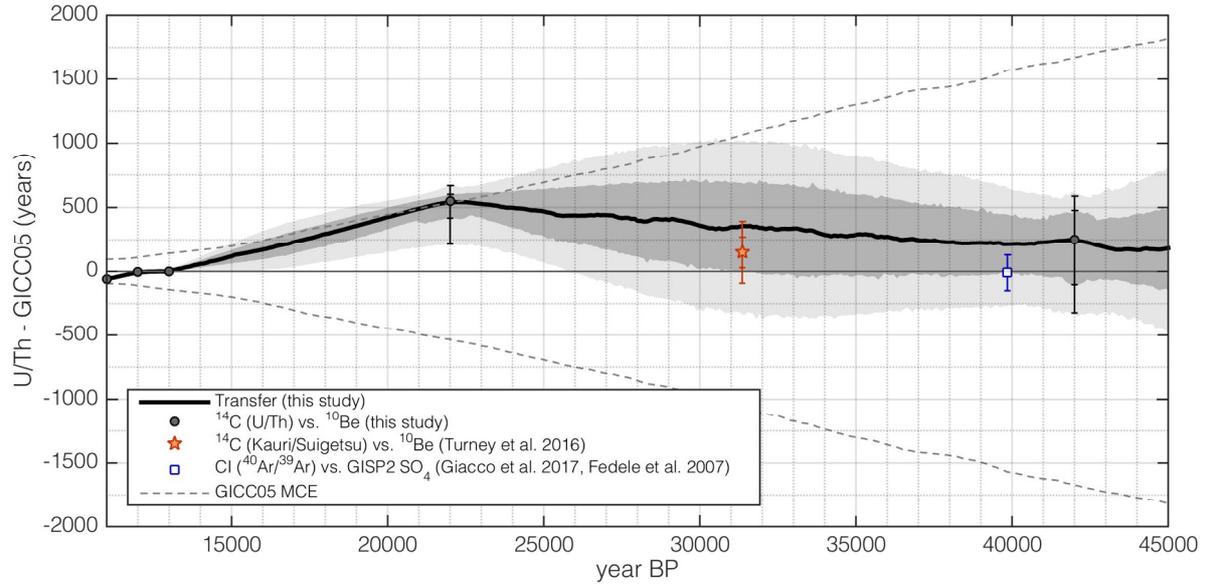
Figure 12: Transfer function between the U/Th timescale and GICC05. The transfer function is shown in black with dark and light grey shading encompassing its 68.2% and 95.4% confidence intervals. The black dots with error bars show the used match points between ^{14}C and ^{10}Be. The red star shows the difference between ages of a glacial kauri tree ^{14}C sequence on Lake Suigetsu ^{14}C and GRIP ^{10}Be (Turney et al., 2016). The blue open square shows the age difference between the ^{40}Ar/^{39}Ar-age of the Campanian Ignimbrite (Giaccio et al., 2017), and a tentatively associated spike in the GISP2 SO$_4$ record (Fedele et al., 2007) on the GICC05 timescale (Seierstad et al., 2014).

5 The timing of DO-events

To investigate the synchroneity of climate changes recorded in different parts of the globe, we compare ice-core data to a selection of well-dated speleothem records. The well-known Hulu-Dongge Cave records have become iconic blueprints for intensity changes of the East Asian Summer Monsoon (EASM) anchored on a precise U/Th timescale (Cheng et al., 2016; Dykoski et al., 2005; Wang et al., 2001). The speleothem records from Cueva del Diamante and El Condor reflect changes in precipitation amount over eastern Amazonia associated with the South American Monsoon (Cheng et al., 2013b). The speleothem records from Sofular Cave, Turkey, are not straightforward in their mechanistic interpretation but likely reflect a mix of temperature and seasonality of precipitation (δ^{18}O), and type and density of vegetation, soil microbial activity (δ^{13}C), and hence, effective moisture and temperature (Fleitmann et al., 2009). Hence, while this list of speleothem data can certainly be expanded in future studies, we chose these four speleothem records from 3 different regions that are all well-dated and sensitive to the position of the ITCZ and compare it to the ice-core records. We used the NGRIP Ca record (Bigler, 2004), that shows the largest signal to noise ratio across DO-events (compared to e.g., δ^{18}O) making their identification more precise. In addition, the Ca aerosols originate from Asian dust sources (Svensson et al., 2000) and are thus, more directly related to Asian hydroclimate (Schüpbach et al., 2018) making them potentially more comparable to for example the Hulu cave record. Potential phasing differences between different climate proxies in the ice core are small compared to our synchronization uncertainties (Steffensen et al., 2008).

634
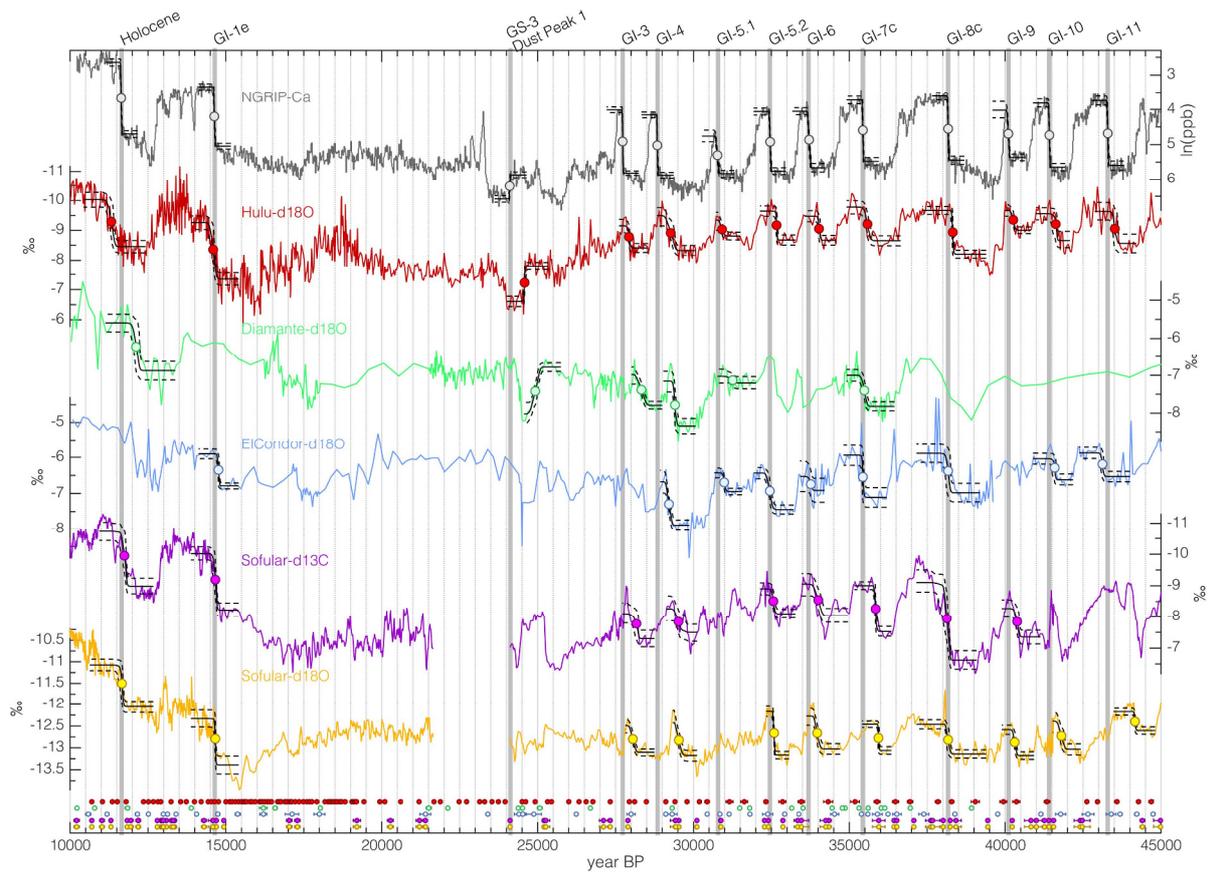
Figure 13: Timing of abrupt climate changes in different climate records. The climate archive and proxy is indicated in each panel. The black lines show the mean of the fitted ramps and their 95% confidence intervals (dashed). The dots mark the midpoint of the mean transition. The U/Th dates and their ±1σ uncertainties of each climate record are shown at the bottom of the figure in colour coding corresponding to the respective climate record. Each time series is shown on its original timescale not applying any synchronization.

640

Figure 13 shows the ice-core and speleothem climate records on their original individual timescales, along with the fitted ramps to the rapid climate changes. Note that we could not fit each climate event for every record, since the method requires a minimum number of data points defining the levels before and after each transition to produce reliable estimates. Already visually, a lag of climate changes in Greenland compared to the speleothem records can be consistently identified between 20 and 35 ka BP when all records are on their original timescales. Combining the PDFs of the detected change points in Greenland and the speleothems allows us to infer a probability estimate of the timing difference between climate events in Greenland and speleothems. These differences are shown in figure 14 along with our transfer function based on the matching of radionuclides from figure 12. This comparison shows that the differences in the timing of start-, mid- and end-point of DO-events in speleothems and ice cores largely fall within the uncertainties of our radionuclide-based timescale transfer function. Thus, rapid climate changes occur synchronously in Greenland and the (sub-) tropics. Notable exceptions are i) the transition from GS-1 to the Holocene around 11.6 ka BP, ii) Heinrich event 2 at 24 ka BP, and iii) DO-11 around 43 ka BP. However, there is large scatter among the different speleothem-based estimates at these events, indicating that these events are asynchronous in the different speleothems records on their respective timescales. Consequently, some of these records also imply asynchronous climate shifts with Greenland ice cores. This may either be interpreted as an indication of time-transgressive climate

657 changes, or as a bias in individual speleothems – either in how climate is recorded in the speleothem, or their
658 dating (for example through detrital thorium).
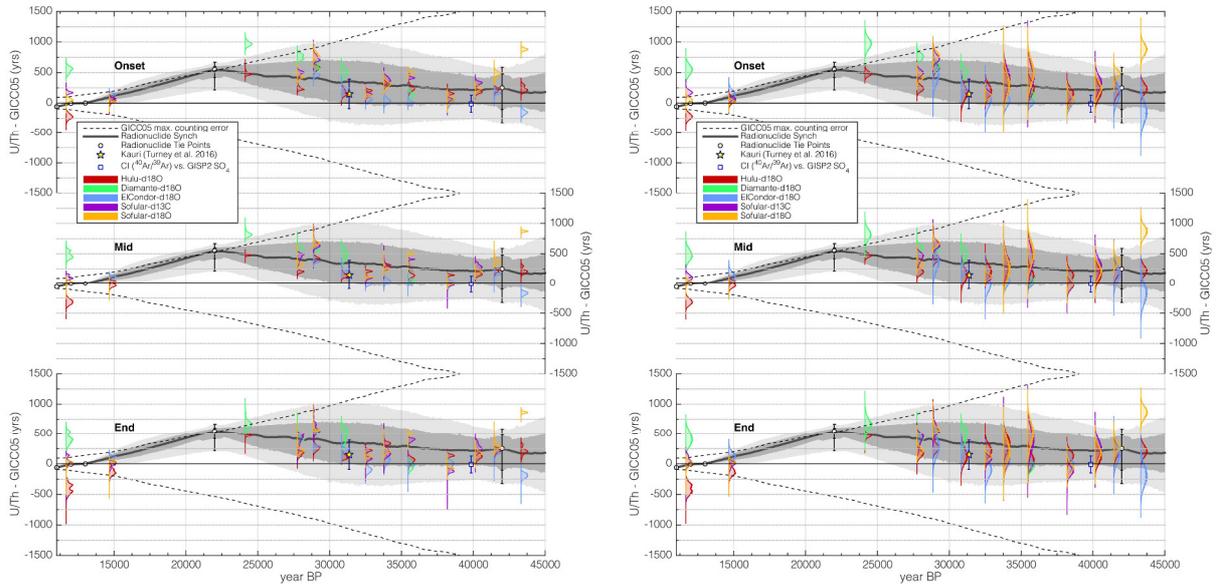
Figure 14: Timing differences of the onset (top), midpoint (middle) and end (bottom) of rapid climate changes in NGRIP and speleothems (coloured PDFs, see legend), and the timescale transfer function inferred from radionuclide matching (black line and grey shadings as in figure 12). The left panels show the PDFs of timing differences including only uncertainties from the determination of the change points in the climate records, while the right hand panels also include the speleothem dating uncertainties.

665 Averaging over all DO events, we can estimate an overall probability of leads and lags. By using the individual
666 realizations of the radionuclide-based transfer function (see section 4.4) we take into account that the
667 uncertainties of the transfer function are strongly autocorrelated. For each realization, we randomly sample the
668 PDFs for the onset of the DO-events for the ice-core and speleothem records (see section 3.5), perturb the
669 speleothem-based estimates within their U/Th dating errors, determine the lead or lag between the DO-onset in
670 ice-core and speleothem records, and correct it for the expected lag from the realization of our transfer function.
671 By averaging over all DO-events we thus obtain a mean lag for each realization and speleothem. In addition, we
672 combine the different speleothem-based estimates of each realization by averaging over their mean lags to
673 obtain an overall (speleothem & DO-event) mean lag. Converting the obtained lags from each realization into
674 histograms we estimate the PDFs of average lags between ice-core and speleothem records.
675 Our lag estimates critically depend on our ability to fill the gaps between the widely spaced tie-points and thus,
676 on our assumptions about the ice-core layer counting uncertainty, and how well our AR(1) process model can
677 capture these (section 4). However, we note that by treating the mce as a highly correlated 1σ (instead of 2σ)
678 uncertainty, our error estimate can be regarded as very conservative since it allows for large systematic drifts in
679 each realization of the transfer function that will result in large errors of the mean.
680 The resulting PDFs of the lag between speleothems and ice cores are shown in figure 15. The uncertainties are
681 mainly determined by our synchronization uncertainty. Thus, the uncertainty is only marginally reduced when
682 averaging over all speleothems (Fig. 15, bottom): Because each realization of the transfer function varies
683 smoothly, the offset between speleothem and ice-core records will be systematic for all speleothems in each
684 realization, and is thus only marginally reduced by averaging.

685 We find that all speleothem records except Cueva del Diamante (Cheng et al., 2013b) indicate synchroneity with

686 NGRIP within 1σ and that the delay obtained for Cueva del Diamante falls within 2σ. We note that the

687 speleothem data from El Condor (Cheng et al., 2013b) from the same region as Cueva del Diamante does not

688 indicate a significant lag to Greenland. Overall, our analysis cannot reject the null-hypothesis of synchronous

689 DO-events in Greenland ice cores and (sub-) tropical speleothems (lag: μ±1σ = 29±189 years).

690
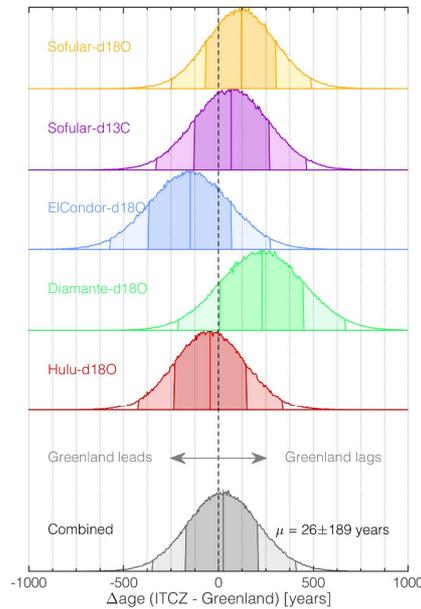
Figure 15: Average lead/lag between the onset of DO-events in the speleothems and NGRIP. Each panel (colour)
shows the PDF for the lead/lag of the onset in the speleothem compared to NGRIP, averaged over all investigated
DO-events (i.e., excluding the GS-3 Dust Peak/H2). The bottom most panel shows the PDF of the average of all DO-
events and speleothems. The dark/light shading of the PDF in each panel indicates 68.2%/95.4% intervals.

6 Discussion

696 Our proposed transfer function quantifies the long-term differences between the Greenland ice-core and U/Th

697 timescale and allows their synchronization. Even though based on only a few tie-points, this can be used to

698 evaluate the absolute dating accuracy of Greenland ice-core records during the past 45 ka BP, while maintaining

699 the strength of their precise relative dating. In combination with similar work done for the Holocene (Adolphi

700 and Muscheler, 2016; Muscheler et al., 2014a), the picture emerges that the GICC05 counting error may be

701 systematic: when accumulation and data resolution is high (e.g. in parts of the Holocene), too many annual

702 layers have been counted, whereas during periods of low accumulation (e.g. GS-1 and GS-2) there is a tendency

703 to identify too few annual layers. In principle, this is well captured by the GICC05 uncertainty estimate as the

704 derivative of our transfer function is (within error) consistent with the increase of the counting error. However,

705 our results caution against the use of the GICC05 counting error as a 2σ uncertainty as is often done in the

706 literature. Originally, Andersen et al. (2006) pointed out that the MCE is not a true σ uncertainty but proposed

707 that a Gaussian distribution with 2σ = MCE could serve as a pragmatic approximation. In combination with

708 results from the Holocene (Adolphi and Muscheler, 2016) our study implies that the counting error can be

709 strongly correlated over extended periods of time. This is in line with the discussion in Rasmussen et al. (2006)

710 who point out that the main contribution to a potential bias in the layer count is the definition of how an annual

711 layer is manifested in the proxy data. The data resolution as well as the manifestation of annual layers change

between different climate states (Rasmussen et al., 2006), likely due to changes in aerosol transport and deposition resulting from variations in the atmospheric circulation and seasonality of precipitation (Merz et al., 2013; Werner et al., 2001). According to our analysis, the largest relative (i.e., year/year) change in the difference between GICC05 and the U/Th and tree-ring timescale occurs over GS-1 (11,653-12,846 years BP) and GS-2 (14,652-23,290 years BP). Both of these periods have likely been characterized by an increased relative contribution of summer precipitation to the annual ice layer (Werner et al., 2000; Denton et al., 2005), and the annual layers in the ice core have been identified in a similar way in both intervals (Rasmussen et al., 2006). In the 11-13 ka BP interval, the offset between GICC05 and the tree-ring timescale changes from -60 (95.4%-range: -77 to -42) years to zero (95.4%-range: -12 to +21) years. During the same interval, the GICC05 maximum counting error grows by 46 years. Albeit consistent within the absolute error margins, this stretch of GICC05 over GS-1 thus slightly exceeds the range allowed by the GICC05 counting error. Muscheler et al. (2014a) discussed that this stretch may be partly explained by errors in the placement of the oldest part of the tree-ring chronologies. However, here, we use a revised late glacial tree-ring dataset in which the different chronologies are connected much more robustly (Hogg et al., 2016). Furthermore, our analysis on the fully independent Hulu Cave ^{14}C data yields similar results (Fig. 7). Hence, our analyses clearly show that the GS-1 interval is about 60 years too short in the GICC05-timescale.

Between 15 and 22 ka BP, our analysis yields a change in the GICC05 offset from +118 (95.4%-range: 2-220) years to +549 (95.4%-range: 207-670) years, while the GICC05 counting error grows by 335 years. Thus, again, our transfer function changes a little faster than the maximum counting error allows during this interval. We note that our ^{14}C-^{10}Be matchpoint around 22,000 years BP has a relatively low signal-to-noise ratio in the ^{14}C data (see Fig. 8-9) and should, thus, be regarded as tentative. However, as shown in figure 8 our results are generally robust against different choices of subsets of the ^{14}C data and time windows. Nevertheless, it can also be seen that the estimates of the most likely age difference (i.e., the peak of the PDFs) differ slightly for different choices of the ^{14}C data. Hulu Cave yields a most likely offset of ~325 years, while Suigetsu implies a bigger age difference of ~550 years that coincides with a secondary probability peak in the Hulu Cave PDF. We note that assuming increased amounts of old soil organic carbon contributing to the speleothem formation would lead to an even stronger difference between these estimates (see section 3.4). Hence, we propose an age difference of +549 (95.4% range: 207-670) years based on the combination of all data (Fig. 9) that is consistent within error with the estimates based on the single datasets shown in figure 8, but stress that this tie-point should be re-evaluated as new suitable ^{14}C data becomes available in the future.

Assuming that the U/Th dates are absolute, our transfer function can be used to account for the bias in the GICC05 timescale and thus facilitate comparisons of ice-core records to other absolutely dated archives. However, we note that our synchronization does not necessarily lead to consistent timescales with radiocarbon-dated records. As discussed in section 3.3.2 (Fig. 4) and section 4.3 (Fig. 10 & 11), discrepancies of the datasets underlying IntCal13 can lead to erroneous structures in the calibration curve. The reduced amplitude of the Δ^{14}C change around the Laschamp geomagnetic field minimum in IntCal13 compared to its underlying data implies that IntCal Δ^{14}C must be offset prior to and/or after the Laschamp event. This underlines the challenges in radiocarbon calibration around this time pointed out by Muscheler et al. (2014b). Also more recently, Giaccio et al. (2017) pointed out that paired ^{40}Ar/^{39}Ar and ^{14}C-dating of the Campanian Ignimbrite around 40 ka BP yields inconsistent ages when the ^{14}C age is calibrated with IntCal13. Since IntCal13 in principle should be tied to the

752 U/Th-age scale for sections older than 13.9 ka BP, this implies either an inconsistency between Ar/Ar and U/Th
753 dating or in the reconstructed ^{14}C levels of the calibration curve. The latter would be congruent with the
754 conclusions by Muscheler et al. (2014b). If the problem was indeed the IntCal ^{14}C reconstruction, a
755 synchronization of ice-core [10]Be to IntCal ^{14}C would not resolve this bias, since the problem would not be one of
756 chronology, but of ^{14}C measurement and/or archive.

757 Our analysis provides the first rigorous test of whether DO-events recorded in speleothems and ice cores occur
758 synchronously. We reject the hypothesis of leads and lags larger than 189 years at the one sigma level,
759 consistent with the findings of Baumgartner et al. (2014). Since we compare to speleothem records from
760 different regions, this also highlights that the ITCZ likely migrated synchronously (within uncertainties) over the
761 different ocean basins and continents during the onset of DO-events (Schneider et al., 2014). However, there are
762 also differences between the different speleothem records, which could be due to limitations in their dating or
763 related to how directly individual archives record the rapid climate changes. The most notable examples are the
764 onset of the Holocene and GI-11, which appear to occur asynchronously in the different speleothems (see Fig.
765 13 & 14). Another example is the younger GS-3 dust peak in the Greenland ice cores that appears to coincide
766 with the East Asian Summer Monsoon decline seen in Hulu Cave, but postdates the precipitation increase seen
767 in El Condor and Diamante. This change in the speleothems is typically attributed to the southward shift of the
768 ITCZ as a response to Heinrich Event 2.

769 Figure 16 shows the period around H2. Firstly, we note that the younger of the two GS-3 dust peaks in the
770 Greenland ice cores (Rasmussen et al., 2014a) occurs coevally (within chronological uncertainty) with the ITCZ
771 movement recorded by the speleothems. At this time, the East Asian Summer Monsoon is strongly reduced as
772 implied by decreased Hulu Cave δ^{18}O (Cheng et al., 2016). Coevally, precipitation increases in the South
773 American Summer Monsoon region (Novello et al., 2017; Stríkis et al., 2018). The records thus exhibit more
774 pronounced stadial conditions than normally seen during (non-Heinrich) DO-events. However, taken at face
775 value, the precipitation increase at El Condor and Cueva del Diamante, the two northernmost sites shown in
776 figure 16 (Cheng et al., 2013b), significantly predates the event seen in Greenland and Hulu Cave. It also
777 predates the more southern South American sites Lapa Sem Fim (Stríkis et al., 2018) and Jaragua (Novello et
778 al., 2017) by more than 500 years. This could either point to errors in the dating of the El Condor and Diamante
779 speleothems, or be related to their latitudinal position. A freshwater-only experiment (all other boundary
780 conditions held constant at 19 ka BP levels) with the Community Climate System Model 3 (TraCE-MWF, He,
781 2011) shows that, during a weak AMOC state, reduced advection of moisture from the tropical Atlantic leads to
782 lower precipitation north of the ITCZ, while the ITCZ position over South America itself changes very little
783 (Fig. 16). El Condor and Cueva del Diamante are both located very close to the LGM position of the ITCZ. It is
784 hence possible, that when northern hemisphere summer insolation reached its lowest values over the past 50
785 kaBP around H2, the ITCZ migrated to a position south of El Condor and Cueva del Diamante, and during its
786 transition caused the reconstructed precipitation change. As a result, the precipitation response to freshwater
787 forcing would change sign at these cave sites. The sites located slightly further south only show a weak
788 (Pacupahuain) or no (Paixao) response during this period, but are both characterized by increased variability.
789 The two southernmost sites on the other hand (Jaragua and Lapa Sem Fim) remain south of the ITCZ
790 throughout, and hence, show a clear increase in precipitation coeval with the signal in Greenland and Hulu
791 Cave. In this context, the precipitation increase in El Condor and Cueva del Diamante around 25kaBP (i.e., prior

to H2) may signify when the ITCZ transitions over the sites. The subsequent reduction in AMOC strength during H2 then leads to a decrease in precipitation in north-west South America, an increase further south, and little change in between. Tentative support for this can be drawn from the response of the El Condor and Cueva del Diamante speleothems to GI-2.2 and GI-2.1 where, albeit weakly, the δ^{18}O records imply an increase in precipitation during GI-2 which is opposite to their response to DO-events during MIS-3 (Fig. 13, 16). Thus, this analysis indicates, that the seemingly asynchronous response to climate change in different proxy records may indeed only reflect site specific changes in the proxy response. Alternatively, we cannot rule out undetected issues with the U/Th ages of these speleothems. A detailed analysis of this observation feature is beyond the scope of this paper, but in the context of a timescale perspective, which is the focus of this work, it highlights the caveats of climate wiggle-matching between single records, even if the mechanistic link between regional climate changes may be relatively well understood.
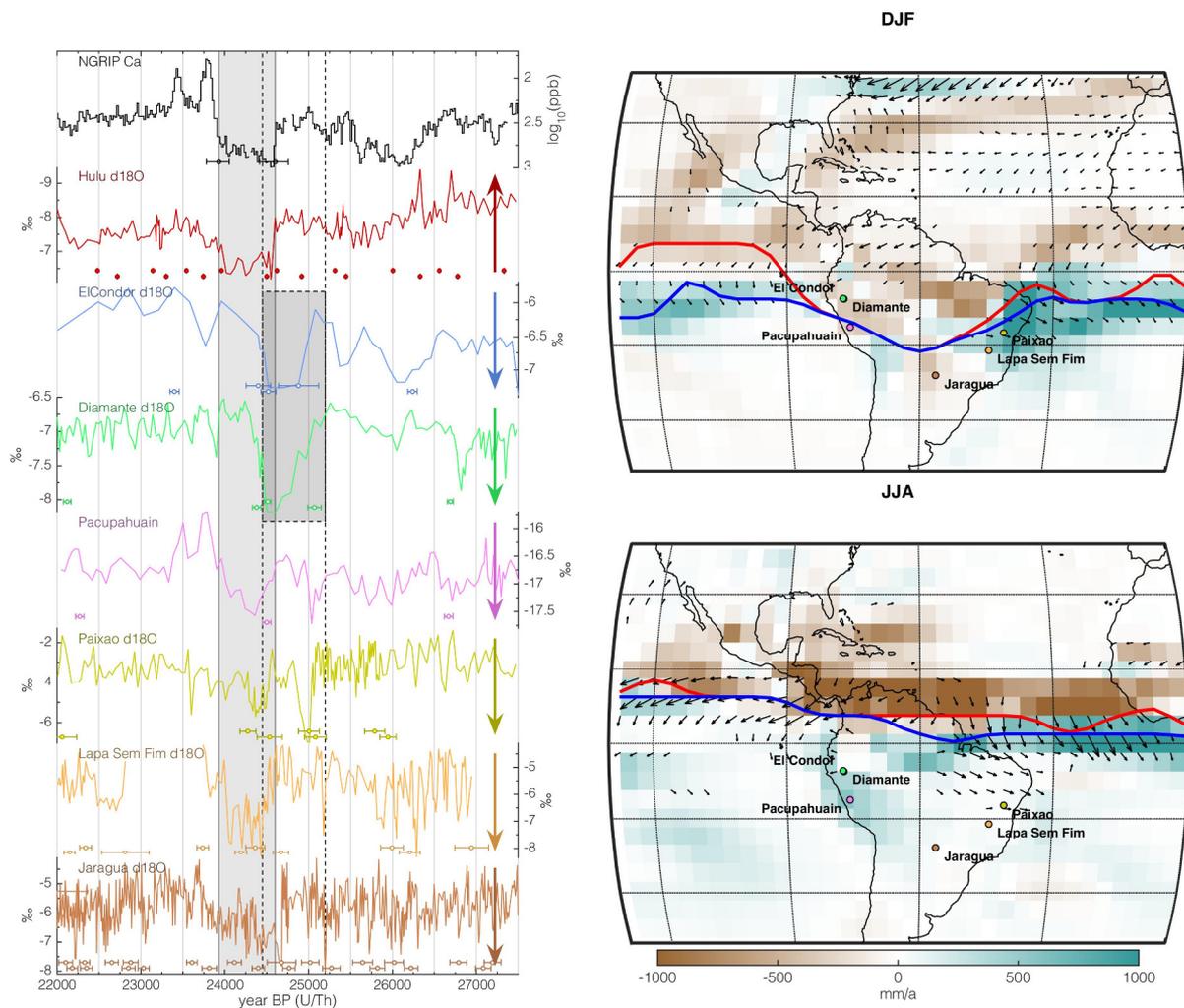
Figure 16: Climate changes around H2. Left (from top to bottom): NGRIP Ca (Bigler, 2004) on the synchronized timescale (Fig. 14), Hulu Cave δ^{18}O (Cheng et al., 2016), El Condor δ^{18}O (Cheng et al., 2013b), Cueva del Diamante δ^{18}O (Cheng et al., 2013b), Pacupahuain δ^{18}O (Kanner et al., 2012), Paixao δ^{18}O (Stríkis et al., 2018), Lapa Sem Fim δ^{18}O (Stríkis et al., 2018), Jaragua Cave δ^{18}O (Novello et al., 2017). The arrows on the right hand side of each axis point in the direction of the signature of increased precipitation on δ^{18}O through the amount effect (Dansgaard, 1964). The light grey box marks H2. The dark grey box highlights the preceding δ^{18}O anomaly in El Condor and Diamante caves. Right: Precipitation (colour) and wind (arrows) response to freshwater forcing in the CCSM3 climate model (freshwater only experiment of TraCE21k, all other forcings are held at 19k conditions, He, 2011). The red (blue) line depicts the latitude of the precipitation maximum during strong (weak) AMOC-states. Only wind anomalies >1m/s are plotted. The cave sites are indicated as dots. The top panel shows the winter (December-

February) response, while the bottom panel shows the summer (June-August) response. Anomalies are plotted as weak-strong AMOC mode.

803

7 Conclusion

805 We present the first radionuclide-based comparison between the Greenland Ice Core Chronology 2005
806 (GICC05) and the U/Th timescale. We find that GICC05 is accurate within its stated absolute uncertainties, but
807 also that the maximum counting error of the GICC05 may be at the limit to capture the total uncertainty
808 accumulated within certain climatic periods. Our analysis indicates that the relationship between GICC05 and
809 the U/Th timescale over the last 45 ka drifts over time and reaches its maximum offset around 22 ka BP. We
810 propose a transfer function that quantifies this drift and facilitates analysis of ice-core and U/Th records, such as
811 speleothems, on a common time scale. Thus, this transfer function allows further integration of key-timescales
812 in paleosciences and contributes to the INTIMATE (INTegration of Ice-core, MArine, and TErrestrial records)
813 initiative (Bjorck et al., 1996; Rasmussen et al., 2014b; Bronk Ramsey et al., 2014). Provided that U/Th ages are
814 regarded accurate, the transfer function strongly reduces the absolute dating uncertainty of Greenland ice cores
815 back to 45 ka BP. We reject the hypothesis if leads or lags larger than 189 years between Greenland, East Asia,
816 and South America at the one sigma level. We show that the southward ITCZ shift around 24.5 ka BP seen in
817 speleothems, typically associated with H2, coincides with the younger GS-3 dust peak recorded in Greenland ice
818 cores. However, we also highlight inconsistencies between speleothem records around the onset of the
819 Holocene, late GS-3, and GI-11 and thus, caveats to the commonly applied practice of climate wiggle-matching.
820 By comparing various ^{14}C records underlying IntCal13 as well as ice-core [10]Be data and geomagnetic field
821 records, we infer that the current radiocarbon calibration curve underestimates the amplitude and rapidity of the
822 $\Delta^{14}C$ change around the Laschamp event 41 ka BP. This adds to previous studies (Giaccio et al., 2017;
823 Muscheler et al., 2014b) highlighting that there are likely systematic errors in IntCal13 that will directly
824 translate into errors of radiocarbon-based chronologies around that time. The combination of several internally
825 inconsistent datasets in IntCal13 can lead to erroneous timing and amplitude of $\Delta^{14}C$ changes. Hence, great care
826 has to be taken when attempting to use sections older than 30 ka BP of IntCal13 directly for studies of [14]C
827 production rates and/or carbon cycle changes.

8 Data Availability

829 The transfer function shown in figure 12 will be made available as a supplementary to this paper and on NOAA.

9 Author contributions

831 FA designed and carried out analyses, and wrote the manuscript in correspondence with CBR and RM. TE
832 designed and applied break-point detection analysis and wrote the corresponding methods section. FA, RM,
833 CBR, SOR, CT and AC initiated the project. RLE and HC provided speleothem data. AS and SOR provided
834 insights into the ice core chronology. HF and TE gave insights into aerosol transport and deposition. All authors
835 discussed and commented on the manuscript.

10 Competing interests

The authors declare that they have no conflict of interest.

11 Acknowledgements

FA was supported through a grant by the Swedish Research Council to FA (Vetenskapsrådet DNr. 2016-00218). CBR was partially supported through the UK Natural Environment Research Council (NERC) Radiocarbon Facility (NRCF010002). TE and HF acknowledge the long-term support of ice-core research at the University of Bern by the Swiss National Science Foundation (SNSF) and the Oeschger Center for Climate Change Research. SOR gratefully acknowledges support from the Carlsberg Foundation to the project ChronoClimate. This work was partially supported by the Swedish Research Council (grant DNR2013-8421 to RM), the NSF 1702816 to RLE, and the Australian Research Council DP170104665 to CT and AC. We gratefully acknowledge the financial support of the University of Adelaide Environment Institute, for the initial Marble Hill meeting that initiated this work.

References

Adolphi, F., Muscheler, R., Svensson, A., Aldahan, A., Possnert, G., Beer, J., Sjolte, J., Björck, S., Matthes, K., and Thiéblemont, R.: Persistent link between solar activity and Greenland climate during the Last Glacial Maximum, Nat Geosci, 7, 662-666, 10.1038/ngeo2225, 2014.

Adolphi, F., and Muscheler, R.: Synchronizing the Greenland ice core and radiocarbon timescales over the Holocene – Bayesian wiggle-matching of cosmogenic radionuclide records, Clim. Past, 12, 15-30, 10.5194/cp-12-15-2016, 2016.

Adolphi, F., Muscheler, R., Friedrich, M., Güttler, D., Wacker, L., Talamo, S., and Kromer, B.: Radiocarbon calibration uncertainties during the last deglaciation: Insights from new floating tree-ring chronologies, Quaternary Sci Rev, 170, 98-108, https://doi.org/10.1016/j.quascirev.2017.06.026, 2017.

Andersen, K. K., Azuma, N., Barnola, J. M., Bigler, M., Biscaye, P., Caillon, N., Chappellaz, J., Clausen, H. B., Dahl-Jensen, D., Fischer, H., Fluckiger, J., Fritzsche, D., Fujii, Y., Goto-Azuma, K., Gronvold, K., Gundestrup, N. S., Hansson, M., Huber, C., Hvidberg, C. S., Johnsen, S. J., Jonsell, U., Jouzel, J., Kipfstuhl, S., Landais, A., Leuenberger, M., Lorrain, R., Masson-Delmotte, V., Miller, H., Motoyama, H., Narita, H., Popp, T., Rasmussen, S. O., Raynaud, D., Rothlisberger, R., Ruth, U., Samyn, D., Schwander, J., Shoji, H., Siggard-Andersen, M. L., Steffensen, J. P., Stocker, T., Sveinbjornsdottir, A. E., Svensson, A., Takata, M., Tison, J. L., Thorsteinsson, T., Watanabe, O., Wilhelms, F., White, J. W., and North Greenland Ice Core Project, m.: High-resolution record of Northern Hemisphere climate extending into the last interglacial period, Nature, 431, 147-151, 10.1038/nature02805, 2004.

Andersen, K. K., Svensson, A., Johnsen, S. J., Rasmussen, S. O., Bigler, M., Röthlisberger, R., Ruth, U., Siggaard-Andersen, M.-L., Peder Steffensen, J., and Dahl-Jensen, D.: The Greenland Ice Core Chronology 2005, 15–42ka. Part 1: constructing the time scale, Quaternary Sci Rev, 25, 3246-3257, 10.1016/j.quascirev.2006.08.002, 2006.

873 Bard, E., Raisbeck, G. M., Yiou, F., and Jouzel, J.: Solar modulation of cosmogenic nuclide production
874 over the last millennium: comparison between 14C and 10Be records, Eart Planet Sc Lett, 150, 453-
875 462, 10.1016/s0012-821x(97)00082-4, 1997.

876 Bard, E., Arnold, M., Hamelin, B., Tisnerat-Laborde, N., and Cabioch, G.: Radiocarbon Calibration by
877 Means of Mass Spectrometric 230Th/234U and 14C Ages of Corals: An Updated Database Including
878 Samples from Barbados, Mururoa and Tahiti, Radiocarbon, 40, 1085-1092,
879 10.1017/S0033822200019135, 1998.

880 Bard, E., Ménot, G., Rostek, F., Licari, L., Böning, P., Edwards, R. L., Cheng, H., Wang, Y., and Heaton,
881 T. J.: Radiocarbon calibration/comparison records based on marine sediments from the Pakistan and
882 Iberian margins, Radiocarbon, 55, 1999-2019, 2013.

883 Baumgartner, M., Kindler, P., Eicher, O., Floch, G., Schilt, A., Schwander, J., Spahni, R., Capron, E.,
884 Chappellaz, J., Leuenberger, M., Fischer, H., and Stocker, T. F.: NGRIP CH4 concentration from 120 to
885 10 kyr before present and its relation to a δ15N temperature reconstruction from the same ice core,
886 Clim. Past, 10, 903-920, 10.5194/cp-10-903-2014, 2014.

887 Baumgartner, S., Beer, J., Suter, M., Dittrich-Hannen, B., Synal, H. A., Kubik, P. W., Hammer, C., and
888 Johnsen, S.: Chlorine 36 fallout in the Summit Greenland Ice Core Project ice core, Journal of
889 Geophysical Research: Oceans, 102, 26659-26662, 10.1029/97JC00166, 1997a.

890 Baumgartner, S., Beer, J., Wagner, G., Kubik, P., Suter, M., Raisbeck, G. M., and Yiou, F.: 10Be and
891 dust, Nuclear Instruments and Methods in Physics Research Section B: Beam Interactions with
892 Materials and Atoms, 123, 296-301, 10.1016/s0168-583x(96)00751-3, 1997b.

893 Baumgartner, S., Beer, J., Masarik, J., Wagner, G., Meynadier, L., and Synal, H.-A.: Geomagnetic
894 Modulation of the 36Cl Flux in the GRIP Ice Core, Greenland, Science, 279, 1330-1332,
895 10.1126/science.279.5355.1330, 1998.

896 Bigler, M.: Hochauflösende Spurenstoffmessungen an polaren Eisbohrkernen: Glazio-chemische und
897 klimatische Prozessstudien, PhD, Environmental Physics, University of Bern, Bern, 2004.

898 Bjorck, S., Kromer, B., Johnsen, S., Bennike, O., Hammarlund, D., Lemdahl, G., Possnert, G.,
899 Rasmussen, T. L., Wohlfarth, B., Hammer, C. U., and Spurk, M.: Synchronized TerrestrialAtmospheric
900 Deglacial Records Around the North Atlantic, Science, 274, 1155-1160,
901 10.1126/science.274.5290.1155, 1996.

902 Bourne, A. J., Davies, S. M., Abbott, P. M., Rasmussen, S. O., Steffensen, J. P., and Svensson, A.:
903 Revisiting the Faroe Marine Ash Zone III in two Greenland ice cores: implications for marine‐ice
904 correlations, Journal of Quaternary Science, 28, 641-646, doi:10.1002/jqs.2663, 2013.

905 Broecker, W. S.: A preliminary evaluation of uranium series inequilibrium as a tool for absolute age
906 measurement on marine carbonates, J Geophys Res, 68, 2817-2834, 10.1029/JZ068i009p02817,
907 1963.

908 Bronk Ramsey, C., van der Plicht, J., and Weninger, B.: " Wiggle matching" radiocarbon dates,
909 Radiocarbon, 43, 381-390, 2001.

910 Bronk Ramsey, C., Staff, R. A., Bryant, C. L., Brock, F., Kitagawa, H., van der Plicht, J., Schlolaut, G.,
911 Marshall, M. H., Brauer, A., Lamb, H. F., Payne, R. L., Tarasov, P. E., Haraguchi, T., Gotanda, K.,
912 Yonenobu, H., Yokoyama, Y., Tada, R., and Nakagawa, T.: A complete terrestrial radiocarbon record
913 for 11.2 to 52.8 kyr B.P, Science, 338, 370-374, 10.1126/science.1226660, 2012.

914 Bronk Ramsey, C., Albert, P., Blockley, S., Hardiman, M., Lane, C., Macleod, A., Matthews, I. P.,
915 Muscheler, R., Palmer, A., and Staff, R. A.: Integrating timescales with time-transfer functions: a
916 practical approach for an INTIMATE database, Quaternary Sci Rev, 106, 67-80,
917 10.1016/j.quascirev.2014.05.028, 2014.

918 Buizert, C., Adrian, B., Ahn, J., Albert, M., Alley, R. B., Baggenstos, D., Bauska, T. K., Bay, R. C.,
919 Bencivengo, B. B., Bentley, C. R., Brook, E. J., Chellman, N. J., Clow, G. D., Cole-Dai, J., Conway, H.,
920 Cravens, E., Cuffey, K. M., Dunbar, N. W., Edwards, J. S., Fegyveresi, J. M., Ferris, D. G., Fitzpatrick, J.
921 J., Fudge, T. J., Gibson, C. J., Gkinis, V., Goetz, J. J., Gregory, S., Hargreaves, G. M., Iverson, N.,
922 Johnson, J. A., Jones, T. R., Kalk, M. L., Kippenhan, M. J., Koffman, B. G., Kreutz, K., Kuhl, T. W., Lebar,
923 D. A., Lee, J. E., Marcott, S. A., Markle, B. R., Maselli, O. J., McConnell, J. R., McGwire, K. C., Mitchell,
924 L. E., Mortensen, N. B., Neff, P. D., Nishiizumi, K., Nunn, R. M., Orsi, A. J., Pasteris, D. R., Pedro, J. B.,
925 Pettit, E. C., Price, P. B., Priscu, J. C., Rhodes, R. H., Rosen, J. L., Schauer, A. J., Schoenemann, S. W.,
926 Sendelbach, P. J., Severinghaus, J. P., Shturmakov, A. J., Sigl, M., Slawny, K. R., Souney, J. M., Sowers,
927 T. A., Spencer, M. K., Steig, E. J., Taylor, K. C., Twickler, M. S., Vaughn, B. H., Voigt, D. E., Waddington,
928 E. D., Welten, K. C., Wendricks, A. W., White, J. W. C., Winstrup, M., Wong, G. J., and Woodruff, T. E.:
929 Precise interpolar phasing of abrupt climate change during the last ice age, Nature, 520, 661-665,
930 10.1038/nature14401
931 http://www.nature.com/nature/journal/v520/n7549/abs/nature14401.html#supplementary-
932 information, 2015.

933 Cauquoin, A., Raisbeck, G. M., Jouzel, J., and Paillard, D.: Use of 10Be to Predict Atmospheric 14C
934 Variations during the Laschamp Excursion: High Sensitivity to Cosmogenic Isotope Production
935 Calculations, Radiocarbon, 56, 67-82, 10.2458/56.16478, 2014.

936 Cheng, H., Lawrence Edwards, R., Shen, C.-C., Polyak, V. J., Asmerom, Y., Woodhead, J., Hellstrom, J.,
937 Wang, Y., Kong, X., Spötl, C., Wang, X., and Calvin Alexander Jr, E.: Improvements in 230Th dating,
938 230Th and 234U half-life values, and U–Th isotopic measurements by multi-collector inductively
939 coupled plasma mass spectrometry, Eart Planet Sc Lett, 371–372, 82-91,
940 http://dx.doi.org/10.1016/j.epsl.2013.04.006, 2013a.

941 Cheng, H., Sinha, A., Cruz, F. W., Wang, X., Edwards, R. L., d'Horta, F. M., Ribas, C. C., Vuille, M., Stott,
942 L. D., and Auler, A. S.: Climate change patterns in Amazonia and biodiversity, Nat Commun, 4, 1411,
943 10.1038/ncomms2415
944 https://www.nature.com/articles/ncomms2415#supplementary-information, 2013b.

945 Cheng, H., Edwards, R. L., Sinha, A., Spötl, C., Yi, L., Chen, S., Kelly, M., Kathayat, G., Wang, X., Li, X.,
946 Kong, X., Wang, Y., Ning, Y., and Zhang, H.: The Asian monsoon over the past 640,000 years and ice
947 age terminations, Nature, 534, 640-646, 10.1038/nature18591
948 http://www.nature.com/nature/journal/v534/n7609/abs/nature18591.html#supplementary-
949 information, 2016.

950 Craig, H.: The Natural Distribution of Radiocarbon and the Exchange Time of Carbon Dioxide
951 Between Atmosphere and Sea, Tellus, 9, 1-17, 10.1111/j.2153-3490.1957.tb01848.x, 1957.

952 Cutler, K., Gray, S., Burr, G., Edwards, R., Taylor, F., Cabioch, G., Beck, J., Cheng, H., and Moore, J.:
953 Radiocarbon calibration and comparison to 50 kyr BP with paired 14C and 230Th dating of corals
954 from Vanuatu and Papua New Guinea, Radiocarbon, 46, 1127-1160, 2004.

955 Dansgaard, W.: Stable isotopes in precipitation, Tellus, 16, 436-468, doi:10.1111/j.2153-
956 3490.1964.tb00181.x, 1964.

957 Dansgaard, W., and Johnsen, S. J.: A Flow Model and a Time Scale for the Ice Core from Camp
958 Century, Greenland, Journal of Glaciology, 8, 215-223, 10.3189/S0022143000031208, 1969.

959 Dansgaard, W., Johnsen, S. J., Møller, J., and Langway, C. C.: One Thousand Centuries of Climatic
960 Record from Camp Century on the Greenland Ice Sheet, Science, 166, 377-380,
961 10.1126/science.166.3903.377, 1969.

962 Dansgaard, W., Johnsen, S. J., Clausen, H. B., Dahl-Jensen, D., Gundestrup, N. S., Hammer, C. U.,
963 Hvidberg, C. S., Steffensen, J. P., Sveinbjörnsdottir, A. E., Jouzel, J., and Bond, G.: Evidence for
964 general instability of past climate from a 250-kyr ice-core record, Nature, 364, 218,
965 10.1038/364218a0, 1993.

966 Delmas, R. J., Beer, J., Synal, H.-A., Muscheler, R., Petit, J.-R., and Pourchet, M.: Bomb-test 36Cl
967 measurements in Vostok snow (Antarctica) and the use of 36Cl as a dating tool for deep ice cores,
968 Tellus B, 56, 492-498, doi:10.1111/j.1600-0889.2004.00109.x, 2004.

969 Denton, G., Alley, R., Comer, G., and Broecker, W.: The role of seasonality in abrupt climate change,
970 Quaternary Sci Rev, 24, 1159-1182, 10.1016/j.quascirev.2004.12.002, 2005.

971 Durand, N., Deschamps, P., Bard, E., Hamelin, B., Camoin, G., Thomas, A. L., Henderson, G. M.,
972 Yokoyama, Y., and Matsuzaki, H.: Comparison of 14C and U-Th Ages in Corals from IODP #310 Cores
973 Offshore Tahiti, Radiocarbon, 55, 1947-1974, 10.2458/azu_js_rc.v55i2.16134, 2013.

974 Dykoski, C. A., Edwards, R. L., Cheng, H., Yuan, D., Cai, Y., Zhang, M., Lin, Y., Qing, J., An, Z., and
975 Revenaugh, J.: A high-resolution, absolute-dated Holocene and deglacial Asian monsoon record from
976 Dongge Cave, China, Eart Planet Sc Lett, 233, 71-86, https://doi.org/10.1016/j.epsl.2005.01.036,
977 2005.

978 Edwards, L. R., CHEN, J. H., Ku, T.-L., and Wasserburg, G. J.: Precise Timing of the Last Interglacial
979 Period from Mass Spectrometric Determination of Thorium-230 in Corals, Science, 236, 1547-1553,
980 10.1126/science.236.4808.1547, 1987.

981 Efron, B.: Bootstrap methods: another look at the jackknife, The annals of Statistics, 1-26, 1979.

982 Eggleston, S., Schmitt, J., Bereiter, B., Schneider, R., and Fischer, H.: Evolution of the stable carbon
983 isotope composition of atmospheric CO2 over the last glacial cycle, Paleoceanography, 31, 434-452,
984 10.1002/2015PA002874, 2016.

985 Fairbanks, R. G., Mortlock, R. A., Chiu, T.-C., Cao, L., Kaplan, A., Guilderson, T. P., Fairbanks, T. W.,
986 Bloom, A. L., Grootes, P. M., and Nadeau, M.-J.: Radiocarbon calibration curve spanning 0 to 50,000

987   years BP based on paired 230Th/234U/238U and 14C dates on pristine corals, Quaternary Sci Rev,
988   24, 1781-1796, 10.1016/j.quascirev.2005.04.007, 2005.

989   Fedele, F. G., Giaccio, B., Isaia, R., Orsi, G., Carroll, M., and Scaillet, B.: The Campanian Ignimbrite
990   factor: towards a reappraisal of the Middle to Upper Palaeolithic 'transition', Living under the
991   shadow: cultural impacts of volcanic eruptions, 19-41, 2007.

992   Field, C. V., Schmidt, G. A., Koch, D., and Salyk, C.: Modeling production and climate-related impacts
993   on10Be concentration in ice cores, J Geophys Res, 111, D15107, 10.1029/2005jd006410, 2006.

994   Finkel, R. C., and Nishiizumi, K.: Beryllium 10 concentrations in the Greenland Ice Sheet Project 2 ice
995   core from 3–40 ka, J Geophys Res, 102, 26699, 10.1029/97jc01282, 1997.

996   Fleitmann, D., Cheng, H., Badertscher, S., Edwards, R. L., Mudelsee, M., Göktürk, O. M., Fankhauser,
997   A., Pickering, R., Raible, C. C., Matter, A., Kramers, J., and Tüysüz, O.: Timing and climatic impact of
998   Greenland interstadials recorded in stalagmites from northern Turkey, Geophys Res Lett, 36, L19707,
999   10.1029/2009GL040050, 2009.

1000   Fohlmeister, J., Kromer, B., and Mangini, A.: The Influence of Soil Organic Matter Age Spectrum on
1001   the Reconstruction of Atmospheric 14C Levels Via Stalagmites, Radiocarbon, 53, 99-115,
1002   10.1017/S003382220003438X, 2011.

1003   Genty, D., and Massault, M.: Carbon transfer dynamics from bomb-14C and δ13C time series of a
1004   laminated stalagmite from SW France—modelling and comparison with other stalagmite records,
1005   Geochimica et Cosmochimica Acta, 63, 1537-1548, https://doi.org/10.1016/S0016-7037(99)00122-2,
1006   1999.

1007   Genty, D., Baker, A., Massault, M., Proctor, C., Gilmour, M., Pons-Branchu, E., and Hamelin, B.: Dead
1008   carbon in stalagmites: carbonate bedrock paleodissolution vs. ageing of soil organic matter.
1009   Implications for 13C variations in speleothems, Geochimica et Cosmochimica Acta, 65, 3443-3457,
1010   https://doi.org/10.1016/S0016-7037(01)00697-4, 2001.

1011   Giaccio, B., Hajdas, I., Isaia, R., Deino, A., and Nomade, S.: High-precision 14C and 40Ar/39Ar dating
1012   of the Campanian Ignimbrite (Y-5) reconciles the time-scales of climatic-cultural processes at 40 ka,
1013   Scientific Reports, 7, 45940, 10.1038/srep45940
1014   https://www.nature.com/articles/srep45940#supplementary-information, 2017.

1015   Gkinis, V., Simonsen, S. B., Buchardt, S. L., White, J. W. C., and Vinther, B. M.: Water isotope diffusion
1016   rates from the NorthGRIP ice core for the last 16,000 years – Glaciological and paleoclimatic
1017   implications, Eart Planet Sc Lett, 405, 132-141, http://dx.doi.org/10.1016/j.epsl.2014.08.022, 2014.

1018   Guillevic, M., Bazin, L., Landais, A., Kindler, P., Orsi, A., Masson-Delmotte, V., Blunier, T., Buchardt, S.
1019   L., Capron, E., Leuenberger, M., Martinerie, P., Prié, F., and Vinther, B. M.: Spatial gradients of
1020   temperature, accumulation and delta18O-ice in Greenland over a series of Dansgaard-Oeschger
1021   events, Clim. Past, 9, 1029-1051, 10.5194/cp-9-1029-2013, 2013.

1022   He, F.: Simulating transient climate evolution of the last deglaciation with CCSM 3, PhD, Atmospheric
1023   and Ocean Sciences, University of Wisconsin-Madison, 185 pp., 2011.

Heikkilä, U., Beer, J., and Feichter, J.: Meridional transport and deposition of atmospheric 10Be, Atmospheric Chemistry and Physics, 9, 515-527, 10.5194/acp-9-515-2009, 2009a.

Heikkilä, U., Beer, J., Feichter, J., Alfimov, V., Synal, H. A., Schotterer, U., Eichler, A., Schwikowski, M., and Thompson, L.: 36Cl bomb peak: comparison of modeled and measured data, Atmos. Chem. Phys., 9, 4145-4156, 10.5194/acp-9-4145-2009, 2009b.

Heikkilä, U., Beer, J., Abreu, J. A., and Steinhilber, F.: On the Atmospheric Transport and Deposition of the Cosmogenic Radionuclides (10Be): A Review, Space Science Reviews, 176, 321-332, 10.1007/s11214-011-9838-0, 2011.

Heikkilä, U., and Smith, A. M.: Production rate and climate influences on the variability of10Be deposition simulated by ECHAM5-HAM: Globally, in Greenland, and in Antarctica, J Geophys Res-Atmos, 118, 2506-2520, 10.1002/jgrd.50217, 2013.

Henry, L. G., McManus, J. F., Curry, W. B., Roberts, N. L., Piotrowski, A. M., and Keigwin, L. D.: North Atlantic ocean circulation and abrupt climate change during the last glaciation, Science, 353, 470-474, 10.1126/science.aaf5529, 2016.

Herbst, K., Muscheler, R., and Heber, B.: The new local interstellar spectra and their influence on the production rates of the cosmogenic radionuclides 10Be and 14C, J Geophys Res, n/a-n/a, 10.1002/2016JA023207, 2016.

Hoffmann, D. L., Beck, J. W., Richards, D. A., Smart, P. L., Singarayer, J. S., Ketchmark, T., and Hawkesworth, C. J.: Towards radiocarbon calibration beyond 28ka using speleothems from the Bahamas, Eart Planet Sc Lett, 289, 1-10, 10.1016/j.epsl.2009.10.004, 2010.

Hogg, A., Southon, J., Turney, C., Palmer, J., Ramsey, C. B., Fenwick, P., Boswijk, G., Büntgen, U., Friedrich, M., Helle, G., Hughen, K., Jones, R., Kromer, B., Noronha, A., Reinig, F., Reynard, L., Staff, R., and Wacker, L.: Decadally Resolved Lateglacial Radiocarbon Evidence from New Zealand Kauri, Radiocarbon, 58, 709-733, 10.1017/RDC.2016.86, 2016.

Hughen, K., Southon, J., Lehman, S., Bertrand, C., and Turnbull, J.: Marine-derived 14C calibration and activity record for the past 50,000 years updated from the Cariaco Basin, Quaternary Sci Rev, 25, 3216-3227, 10.1016/j.quascirev.2006.03.014, 2006.

Johnsen, S. J., Dahl-Jensen, D., Dansgaard, W., and Gundestrup, N.: Greenland palaeotemperatures derived from GRIP bore hole temperature and ice core isotope profiles, Tellus B, 47, 624-629, 10.1034/j.1600-0889.47.issue5.9.x, 1995.

Johnsen, S. J., Dahl-Jensen, D., Gundestrup, N., Steffensen, J. P., Clausen, H. B., Miller, H., Masson-Delmotte, V., Sveinbjörnsdottir, A. E., and White, J.: Oxygen isotope and palaeotemperature records from six Greenland ice-core stations: Camp Century, Dye-3, GRIP, GISP2, Renland and NorthGRIP, Journal of Quaternary Science, 16, 299-307, 10.1002/jqs.622, 2001.

Kanner, L. C., Burns, S. J., Cheng, H., and Edwards, R. L.: High-Latitude Forcing of the South American Summer Monsoon During the Last Glacial, Science, 335, 570-573, 10.1126/science.1213397, 2012.

Köhler, P., Muscheler, R., and Fischer, H.: A model-based interpretation of low-frequency changes in the carbon cycle during the last 120,000 years and its implications for the reconstruction of atmospheric Δ14C, Geochemistry, Geophysics, Geosystems, 7, Q11N06, 10.1029/2005GC001228, 2006.

Laj, C., Kissel, C., Mazaud, A., Channell, J. E. T., and Beer, J.: North Atlantic palaeointensity stack since 75ka (NAPIS-75) and the duration of the Laschamp event, Philos T Roy Soc A, 358, 1009-1025, 10.1098/rsta.2000.0571, 2000.

Laj, C., Kissel, C., and Beer, J.: High Resolution Global Paleointensity Stack Since 75 kyr (GLOPIS-75) Calibrated to Absolute Values, in: Timescales Of The Paleomagnetic Field, American Geophysical Union, 255-265, 2004.

Laj, C., Guillou, H., and Kissel, C.: Dynamics of the earth magnetic field in the 10–75 kyr period comprising the Laschamp and Mono Lake excursions: New results from the French Chaîne des Puys in a global perspective, Eart Planet Sc Lett, 387, 184-197, https://doi.org/10.1016/j.epsl.2013.11.031, 2014.

Lal, D., and Peters, B.: Cosmic Ray Produced Radioactivity on the Earth, in: Kosmische Strahlung II / Cosmic Rays II, edited by: Sitte, K., Handbuch der Physik / Encyclopedia of Physics, Springer Berlin Heidelberg, Berlin Heidelberg, Germany, 551-612, 1967.

Lane, C. S., Brauer, A., Blockley, S. P. E., and Dulski, P.: Volcanic ash reveals time-transgressive abrupt climate change during the Younger Dryas, Geology, 41, 1251-1254, 10.1130/g34867.1, 2013.

Lascu, I., Feinberg, J. M., Dorale, J. A., Cheng, H., and Edwards, R. L.: Age of the Laschamp excursion determined by U-Th dating of a speleothem geomagnetic record from North America, Geology, 44, 139-142, 10.1130/g37490.1, 2016.

Li, T.-Y., Han, L.-Y., Cheng, H., Edwards, R. L., Shen, C.-C., Li, H.-C., Li, J.-Y., Huang, C.-X., Zhang, T.-T., and Zhao, X.: Evolution of the Asian summer monsoon during Dansgaard/Oeschger events 13–17 recorded in a stalagmite constrained by high-precision chronology from southwest China, Quaternary Res, 88, 121-128, 10.1017/qua.2017.22, 2017.

Lougheed, B. C., Filipsson, H. L., and Snowball, I.: Large spatial variations in coastal 14C reservoir age – a case study from the Baltic Sea, Clim. Past, 9, 1015-1028, 10.5194/cp-9-1015-2013, 2013.

Lukasczyk, C. E.: 36Chlor in Grönlandeis, PhD, ETH Zurich, Zurich, Switzerland, 285 pp., 1994.

Markle, B. R., Steig, E. J., Buizert, C., Schoenemann, S. W., Bitz, C. M., Fudge, T. J., Pedro, J. B., Ding, Q., Jones, T. R., White, J. W. C., and Sowers, T.: Global atmospheric teleconnections during Dansgaard-Oeschger events, Nat Geosci, 10, 36-40, 10.1038/ngeo2848 http://www.nature.com/ngeo/journal/v10/n1/abs/ngeo2848.html#supplementary-information, 2016.

Masarik, J., and Beer, J.: Simulation of particle fluxes and cosmogenic nuclide production in the Earth's atmosphere, J Geophys Res-Atmos, 104, 12099-12111, Doi 10.1029/1998jd200091, 1999.

1096   Masarik, J., and Beer, J.: An updated simulation of particle fluxes and cosmogenic nuclide production
1097   in the Earth's atmosphere, J Geophys Res, 114, D11103, 10.1029/2008jd010557, 2009.

1098   Merz, N., Raible, C. C., Fischer, H., Varma, V., Prange, M., and Stocker, T. F.: Greenland accumulation
1099   and its connection to the large-scale atmospheric circulation in ERA-Interim and paleoclimate
1100   simulations, Clim Past, 9, 2433-2450, 10.5194/cp-9-2433-2013, 2013.

1101   Muscheler, R., Beer, J., Wagner, G., Laj, C., Kissel, C., Raisbeck, G. M., Yiou, F., and Kubik, P. W.:
1102   Changes in the carbon cycle during the last deglaciation as indicated by the comparison of 10Be and
1103   14C records, Eart Planet Sc Lett, 219, 325-340, 10.1016/s0012-821x(03)00722-2, 2004.

1104   Muscheler, R., Beer, J., Kubik, P. W., and Synal, H. A.: Geomagnetic field intensity during the last
1105   60,000 years based on 10Be and 36Cl from the Summit ice cores and 14C, Quaternary Sci Rev, 24,
1106   1849-1860, 10.1016/j.quascirev.2005.01.012, 2005.

1107   Muscheler, R., Kromer, B., Björck, S., Svensson, A., Friedrich, M., Kaiser, K. F., and Southon, J.: Tree
1108   rings and ice cores reveal 14C calibration uncertainties during the Younger Dryas, Nat Geosci, 1, 263-
1109   267, 10.1038/ngeo128, 2008.

1110   Muscheler, R., and Heikkilä, U.: Constraints on long-term changes in solar activity from the range of
1111   variability of cosmogenic radionuclide records, Astrophysics and Space Sciences Transactions, 7, 355-
1112   364, 10.5194/astra-7-355-2011, 2011.

1113   Muscheler, R., Adolphi, F., and Knudsen, M. F.: Assessing the differences between the IntCal and
1114   Greenland ice-core time scales for the last 14,000 years via the common cosmogenic radionuclide
1115   variations, Quaternary Sci Rev, 106, 81-87, 10.1016/j.quascirev.2014.08.017, 2014a.

1116   Muscheler, R., Adolphi, F., and Svensson, A.: Challenges in 14C dating towards the limit of the
1117   method inferred from anchoring a floating tree ring radiocarbon chronology to ice core records
1118   around the Laschamp geomagnetic field minimum, Eart Planet Sc Lett, 394, 209-215,
1119   10.1016/j.epsl.2014.03.024, 2014b.

1120   Nakagawa, T., Kitagawa, H., Yasuda, Y., Tarasov, P. E., Nishida, K., Gotanda, K., and Sawai, Y.:
1121   Asynchronous Climate Changes in the North Atlantic and Japan During the Last Termination, Science,
1122   299, 688-691, 10.1126/science.1078235, 2003.

1123   Novello, V. F., Cruz, F. W., Vuille, M., Stríkis, N. M., Edwards, R. L., Cheng, H., Emerick, S., de Paula,
1124   M. S., Li, X., Barreto, E. d. S., Karmann, I., and Santos, R. V.: A high-resolution history of the South
1125   American Monsoon from Last Glacial Maximum to the Holocene, Scientific Reports, 7, 44267,
1126   10.1038/srep44267
1127   https://www.nature.com/articles/srep44267#supplementary-information, 2017.

1128   Nowaczyk, N. R., Frank, U., Kind, J., and Arz, H. W.: A high-resolution paleointensity stack of the past
1129   14   to   68   ka   from   Black   Sea   sediments,   Eart   Planet   Sc   Lett,   384,   1-16,
1130   http://dx.doi.org/10.1016/j.epsl.2013.09.028, 2013.

Pedro, J. B., Heikkilä, U. E., Klekociuk, A., Smith, A. M., van Ommen, T. D., and Curran, M. A. J.: Beryllium-10 transport to Antarctica: Results from seasonally resolved observations and modeling, J Geophys Res-Atmos, 116, n/a-n/a, 10.1029/2011jd016530, 2011.

Pedro, J. B., McConnell, J. R., van Ommen, T. D., Fink, D., Curran, M. A. J., Smith, A. M., Simon, K. J., Moy, A. D., and Das, S. B.: Solar and climate influences on ice core 10Be records from Antarctica and Greenland during the neutron monitor era, Eart Planet Sc Lett, 355-356, 174-186, 10.1016/j.epsl.2012.08.038, 2012.

Poluianov, S. V., Kovaltsov, G. A., Mishev, A. L., and Usoskin, I. G.: Production of cosmogenic isotopes 7Be, 10Be, 14C, 22Na, and 36Cl in the atmosphere: Altitudinal profiles of yield functions, J Geophys Res-Atmos, 121, 8125-8136, 10.1002/2016JD025034, 2016.

Raisbeck, G. M., Yiou, F., Fruneau, M., Loiseaux, J. M., Lieuvin, M., and Ravel, J. C.: Cosmogenic10Be/7Be as a probe of atmospheric transport processes, Geophys Res Lett, 8, 1015-1018, 10.1029/GL008i009p01015, 1981.

Raisbeck, G. M., Yiou, F., Jouzel, J., and Stocker, T. F.: Direct north-south synchronization of abrupt climate change record in ice cores using Beryllium 10, Clim Past, 3, 541-547, 10.5194/cp-3-541-2007, 2007.

Raisbeck, G. M., Cauquoin, A., Jouzel, J., Landais, A., Petit, J. R., Lipenkov, V. Y., Beer, J., Synal, H. A., Oerter, H., Johnsen, S. J., Steffensen, J. P., Svensson, A., and Yiou, F.: An improved north–south synchronization of ice core records around the 41 kyr 10Be peak, Clim. Past, 13, 217-229, 10.5194/cp-13-217-2017, 2017.

Rasmussen, S. O., Andersen, K. K., Svensson, A. M., Steffensen, J. P., Vinther, B. M., Clausen, H. B., Siggaard-Andersen, M. L., Johnsen, S. J., Larsen, L. B., Dahl-Jensen, D., Bigler, M., Röthlisberger, R., Fischer, H., Goto-Azuma, K., Hansson, M. E., and Ruth, U.: A new Greenland ice core chronology for the last glacial termination, J Geophys Res, 111, D06102, 10.1029/2005jd006079, 2006.

Rasmussen, S. O., Seierstad, I. K., Andersen, K. K., Bigler, M., Dahl-Jensen, D., and Johnsen, S. J.: Synchronization of the NGRIP, GRIP, and GISP2 ice cores across MIS 2 and palaeoclimatic implications, Quaternary Sci Rev, 27, 18-28, 10.1016/j.quascirev.2007.01.016, 2008.

Rasmussen, S. O., Abbott, P. M., Blunier, T., Bourne, A. J., Brook, E., Buchardt, S. L., Buizert, C., Chappellaz, J., Clausen, H. B., Cook, E., Dahl-Jensen, D., Davies, S. M., Guillevic, M., Kipfstuhl, S., Laepple, T., Seierstad, I. K., Severinghaus, J. P., Steffensen, J. P., Stowasser, C., Svensson, A., Vallelonga, P., Vinther, B. M., Wilhelms, F., and Winstrup, M.: A first chronology for the North Greenland Eemian Ice Drilling (NEEM) ice core, Clim. Past, 9, 2713-2730, 10.5194/cp-9-2713-2013, 2013.

Rasmussen, S. O., Bigler, M., Blockley, S. P., Blunier, T., Buchardt, S. L., Clausen, H. B., Cvijanovic, I., Dahl-Jensen, D., Johnsen, S. J., Fischer, H., Gkinis, V., Guillevic, M., Hoek, W. Z., Lowe, J. J., Pedro, J. B., Popp, T., Seierstad, I. K., Steffensen, J. P., Svensson, A. M., Vallelonga, P., Vinther, B. M., Walker, M. J. C., Wheatley, J. J., and Winstrup, M.: A stratigraphic framework for abrupt climatic changes during the Last Glacial period based on three synchronized Greenland ice-core records: refining and

extending the INTIMATE event stratigraphy, Quaternary Sci Rev, 106, 14-28, http://dx.doi.org/10.1016/j.quascirev.2014.09.007, 2014a.

Rasmussen, S. O., Birks, H. H., Blockley, S. P. E., Brauer, A., Hajdas, I., Hoek, W. Z., Lowe, J. J., Moreno, A., Renssen, H., Roche, D. M., Svensson, A. M., Valdes, P., and Walker, M. J. C.: Dating, synthesis, and interpretation of palaeoclimatic records of the Last Glacial cycle and model-data integration: advances by the INTIMATE (INTegration of Ice-core, MArine and TErrestrial records) COST Action ES0907, Quaternary Sci Rev, 106, 1-13, http://dx.doi.org/10.1016/j.quascirev.2014.10.031, 2014b.

Reimer, P. J., Bard, E., Bayliss, A., Beck, J. W., Blackwell, P. G., Bronk Ramsey, C., Buck, C. E., Cheng, H., Edwards, R. L., Friedrich, M., Grootes, P. M., Guilderson, T. P., Haflidason, H., Hajdas, I., Hatté, C., Heaton, T. J., Hoffmann, D. L., Hogg, A. G., Hughen, K. A., Kaiser, K. F., Kromer, B., Manning, S. W., Niu, M., Reimer, R. W., Richards, D. A., Scott, E. M., Southon, J. R., Staff, R. A., Turney, C. S. M., and van der Plicht, J.: IntCal13 and Marine13 Radiocarbon Age Calibration Curves 0–50,000 Years cal BP, Radiocarbon, 55, 1869-1887, 10.2458/azu_js_rc.55.16947, 2013.

Roth, R., and Joos, F.: A reconstruction of radiocarbon production and total solar irradiance from the Holocene 14C and CO2 records: implications of data and model uncertainties, Clim Past, 9, 1879-1909, 10.5194/cp-9-1879-2013, 2013.

Schneider, T., Bischoff, T., and Haug, G. H.: Migrations and dynamics of the intertropical convergence zone, Nature, 513, 45-53, 10.1038/nature13636, 2014.

Schüpbach, S., Fischer, H., Bigler, M., Erhardt, T., Gfeller, G., Leuenberger, D., Mini, O., Mulvaney, R., Abram, N. J., Fleet, L., Frey, M. M., Thomas, E., Svensson, A., Dahl-Jensen, D., Kettner, E., Kjaer, H., Seierstad, I., Steffensen, J. P., Rasmussen, S. O., Vallelonga, P., Winstrup, M., Wegner, A., Twarloh, B., Wolff, K., Schmidt, K., Goto-Azuma, K., Kuramoto, T., Hirabayashi, M., Uetake, J., Zheng, J., Bourgeois, J., Fisher, D., Zhiheng, D., Xiao, C., Legrand, M., Spolaor, A., Gabrieli, J., Barbante, C., Kang, J. H., Hur, S. D., Hong, S. B., Hwang, H. J., Hong, S., Hansson, M., Iizuka, Y., Oyabu, I., Muscheler, R., Adolphi, F., Maselli, O., McConnell, J., and Wolff, E. W.: Greenland records of aerosol source and atmospheric lifetime changes from the Eemian to the Holocene, Nat Commun, 9, 1476, 10.1038/s41467-018-03924-3, 2018.

Seierstad, I. K., Abbott, P. M., Bigler, M., Blunier, T., Bourne, A. J., Brook, E., Buchardt, S. L., Buizert, C., Clausen, H. B., Cook, E., Dahl-Jensen, D., Davies, S. M., Guillevic, M., Johnsen, S. J., Pedersen, D. S., Popp, T. J., Rasmussen, S. O., Severinghaus, J. P., Svensson, A., and Vinther, B. M.: Consistently dated records from the Greenland GRIP, GISP2 and NGRIP ice cores for the past 104 ka reveal regional millennial-scale δ18O gradients with possible Heinrich event imprint, Quaternary Sci Rev, 106, 29-46, http://dx.doi.org/10.1016/j.quascirev.2014.10.032, 2014.

Siegenthaler, U., Heimann, M., and Oeschger, H.: 14C variations caused by changes in the global carbon cycle, Radiocarbon, 22, 177-191, 1980.

Singer, B. S., Guillou, H., Jicha, B. R., Laj, C., Kissel, C., Beard, B. L., and Johnson, C. M.: 40Ar/39Ar, K–Ar and 230Th–238U dating of the Laschamp excursion: A radioisotopic tie-point for ice core and climate chronologies, Eart Planet Sc Lett, 286, 80-88, http://dx.doi.org/10.1016/j.epsl.2009.06.030, 2009.

1209   Southon, J.: A First Step to Reconciling the GRIP and GISP2 Ice-Core Chronologies, 0–14,500 yr B.P,
1210   Quaternary Res, 57, 32-37, 10.1006/qres.2001.2295, 2002.

1211   Southon, J., Noronha, A. L., Cheng, H., Edwards, R. L., and Wang, Y.: A high-resolution record of
1212   atmospheric 14C based on Hulu Cave speleothem H82, Quaternary Sci Rev, 33, 32-41,
1213   10.1016/j.quascirev.2011.11.022, 2012.

1214   Staff, R. A., Schlolaut, G., Ramsey, C. B., Brock, F., Bryant, C. L., Kitagawa, H., Van der Plicht, J.,
1215   Marshall, M. H., Brauer, A., and Lamb, H. F.: Integration of the old and new Lake Suigetsu (Japan)
1216   terrestrial radiocarbon calibration data sets, Radiocarbon, 55, 2049-2058, 2013.

1217   Steffensen, J. P., Andersen, K. K., Bigler, M., Clausen, H. B., Dahl-Jensen, D., Fischer, H., Goto-Azuma,
1218   K., Hansson, M., Johnsen, S. J., Jouzel, J., Masson-Delmotte, V., Popp, T., Rasmussen, S. O.,
1219   Rothlisberger, R., Ruth, U., Stauffer, B., Siggaard-Andersen, M. L., Sveinbjornsdottir, A. E., Svensson,
1220   A., and White, J. W.: High-resolution Greenland ice core data show abrupt climate change happens
1221   in few years, Science, 321, 680-684, 10.1126/science.1157707, 2008.

1222   Stríkis, N. M., Cruz, F. W., Barreto, E. A. S., Naughton, F., Vuille, M., Cheng, H., Voelker, A. H. L.,
1223   Zhang, H., Karmann, I., Edwards, R. L., Auler, A. S., Santos, R. V., and Sales, H. R.: South American
1224   monsoon response to iceberg discharge in the North Atlantic, Proceedings of the National Academy
1225   of Sciences, 10.1073/pnas.1717784115, 2018.

1226   Stuiver, M., and Polach, H. A.: Discussion; reporting of C-14 data, Radiocarbon, 19, 355-363, 1977.

1227   Svensson, A., Biscaye, P. E., and Grousset, F. E.: Characterization of late glacial continental dust in the
1228   Greenland Ice Core Project ice core, J Geophys Res-Atmos, 105, 4637-4656,
1229   doi:10.1029/1999JD901093, 2000.

1230   Svensson, A., Andersen, K. K., Bigler, M., Clausen, H. B., Dahl-Jensen, D., Davies, S. M., Johnsen, S. J.,
1231   Muscheler, R., Rasmussen, S. O., and Röthlisberger, R.: The Greenland Ice Core Chronology 2005,
1232   15–42ka. Part 2: comparison to other records, Quaternary Sci Rev, 25, 3258-3267,
1233   10.1016/j.quascirev.2006.08.003, 2006.

1234   Svensson, A., Andersen, K. K., Bigler, M., Clausen, H. B., Dahl-Jensen, D., Davies, S. M., Johnsen, S. J.,
1235   Muscheler, R., Parrenin, F., Rasmussen, S. O., Röthlisberger, R., Seierstad, I., Steffensen, J. P., and
1236   Vinther, B. M.: A 60 000 year Greenland stratigraphic ice core chronology, Clim Past, 4, 47-57,
1237   10.5194/cp-4-47-2008, 2008.

1238   Thomas, Z. A.: Using natural archives to detect climate and environmental tipping points in the Earth
1239   System, Quaternary Sci Rev, 152, 60-71, https://doi.org/10.1016/j.quascirev.2016.09.026, 2016.

1240   Trumbore, S.: AGE OF SOIL ORGANIC MATTER AND SOIL RESPIRATION: RADIOCARBON CONSTRAINTS
1241   ON BELOWGROUND C DYNAMICS, Ecological Applications, 10, 399-411, 10.1890/1051-
1242   0761(2000)010[0399:AOSOMA]2.0.CO;2, 2000.

1243   Turney, C. S. M., Thomas, Z. A., Hutchinson, D. K., Bradshaw, C. J. A., Brook, B. W., England, M. H.,
1244   Fogwill, C. J., Jones, R. T., Palmer, J., Hughen, K. A., and Cooper, A.: Obliquity‐driven expansion of

North Atlantic sea ice during the last glacial, Geophys Res Lett, 42, 10,382-310,390, doi:10.1002/2015GL066344, 2015.

Turney, C. S. M., Palmer, J., Bronk Ramsey, C., Adolphi, F., Muscheler, R., Hughen, K. A., Staff, R. A., Jones, R. T., Thomas, Z. A., Fogwill, C. J., and Hogg, A.: High-precision dating and correlation of ice, marine and terrestrial sequences spanning Heinrich Event 3: Testing mechanisms of interhemispheric change using New Zealand ancient kauri (Agathis australis), Quaternary Sci Rev, 137, 126-134, http://dx.doi.org/10.1016/j.quascirev.2016.02.005, 2016.

Veres, D., Bazin, L., Landais, A., Toyé Mahamadou Kele, H., Lemieux-Dudon, B., Parrenin, F., Martinerie, P., Blayo, E., Blunier, T., Capron, E., Chappellaz, J., Rasmussen, S. O., Severi, M., Svensson, A., Vinther, B., and Wolff, E. W.: The Antarctic ice core chronology (AICC2012): an optimized multi-parameter and multi-site dating approach for the last 120 thousand years, Clim Past, 9, 1733-1748, 10.5194/cp-9-1733-2013, 2013.

Vinther, B. M., Clausen, H. B., Johnsen, S. J., Rasmussen, S. O., Andersen, K. K., Buchardt, S. L., Dahl-Jensen, D., Seierstad, I. K., Siggaard-Andersen, M. L., Steffensen, J. P., Svensson, A., Olsen, J., and Heinemeier, J.: A synchronized dating of three Greenland ice cores throughout the Holocene, J Geophys Res, 111, D13102, 10.1029/2005jd006921, 2006.

Vogt, S., Herzog, G. F., and Reedy, R. C.: Cosmogenic nuclides in extraterrestrial materials, Rev Geophys, 28, 253-275, 10.1029/RG028i003p00253, 1990.

Wagner, G., Masarik, J., Beer, J., Baumgartner, S., Imboden, D., Kubik, P. W., Synal, H. A., and Suter, M.: Reconstruction of the geomagnetic field between 20 and 60 kyr BP from cosmogenic radionuclides in the GRIP ice core, Nuclear Instruments and Methods in Physics Research Section B: Beam Interactions with Materials and Atoms, 172, 597-604, https://doi.org/10.1016/S0168-583X(00)00285-8, 2000.

Wagner, G., Beer, J., Masarik, J., Muscheler, R., Kubik, P. W., Mende, W., Laj, C., Raisbeck, G. M., and Yiou, F.: Presence of the Solar de Vries Cycle (~205 years) during the Last Ice Age, Geophys Res Lett, 28, 303-306, 10.1029/2000gl006116, 2001a.

Wagner, G., Laj, C., Beer, J., Kissel, C., Muscheler, R., Masarik, J., and Synal, H. A.: Reconstruction of the paleoaccumulation rate of central Greenland during the last 75 kyr using the cosmogenic radionuclides 36Cl and 10Be and geomagnetic field intensity data, Eart Planet Sc Lett, 193, 515-521, 10.1016/s0012-821x(01)00504-0, 2001b.

Wang, Y. J., Cheng, H., Edwards, R. L., An, Z. S., Wu, J. Y., Shen, C. C., and Dorale, J. A.: A high-resolution absolute-dated late Pleistocene Monsoon record from Hulu Cave, China, Science, 294, 2345-2348, 10.1126/science.1064618, 2001.

Watson, L. R., Van Doren, J. M., Davidovits, P., Worsnop, D. R., Zahniser, M. S., and Kolb, C. E.: Uptake of HCl molecules by aqueous sulfuric acid droplets as a function of acid concentration, J Geophys Res-Atmos, 95, 5631-5638, doi:10.1029/JD095iD05p05631, 1990.

1281   Werner, M., Mikolajewicz, U., Heimann, M., and Hoffmann, G.: Borehole versus isotope
1282   temperatures on Greenland: Seasonality does matter, Geophys Res Lett, 27, 723-726,
1283   10.1029/1999gl006075, 2000.

1284   Werner, M., Heimann, M., and Hoffmann, G.: Isotopic composition and origin of polar precipitation
1285   in present and glacial climate simulations, Tellus B, 53, 53-71, 10.1034/j.1600-0889.2001.01154.x,
1286   2001.

1287   Yiou, F., Raisbeck, G. M., Baumgartner, S., Beer, J., Hammer, C., Johnsen, S., Jouzel, J., Kubik, P. W.,
1288   Lestringuez, J., Stiévenard, M., Suter, M., and Yiou, P.: Beryllium 10 in the Greenland Ice Core Project
1289   ice core at Summit, Greenland, J Geophys Res, 102, 26783, 10.1029/97jc01265, 1997.

1290   Zerle, L., Faestermann, T., Knie, K., Korschinek, G., Nolte, E., Beer, J., and Schotterer, U.: The 41Ca
1291   bomb pulse and atmospheric transport of radionuclides, J Geophys Res-Atmos, 102, 19517-19527,
1292   10.1029/97JD00701, 1997.
1293